POLITECNICO DI MILANO
School of Industrial and Information Engineering
Department of Energy
Photovoltaic, Power Quality and Lighting System Laboratory
(PhOS)

Comparison and Evaluation of Model-Based State-of-Charge Estimation Algorithms for a Verified Lithium-ion Battery Cell Technology

Master of Science in Electrical Engineering

Supervisor:
Prof. Roberto Sebastiano Faranda

Co-Supervisors:
Dr. Hossein Hafezi
Eng. Naga Venkata Kishore Akkala

Candidate:
Behrooz Nemounehkhah - 904192

Academic Year 2019-2020

To my beloved family, dear friends and instructors who always accepted me for me and supported my dedication, drive, and ambition.

Acknowledgement

With many thanks to Professor Roberto Sebastiano Faranda and Eng. Naga Venkata Kishore Akkala for their consistent support and guidance during this project.
Furthermore, I would like to thank Professor Hannu Laaksonen, Dr. Hossein Hafezi, and MSc. Chethan Parthasarathy from the School of Technology and Innovations, Electrical Engineering, University of Vaasa - Finland for their collaborative and supportive efforts during the project, and providing battery test and modeling data.

Contents

List of Abbreviations

AI	*Artificial Intelligence*
ANSI	*American National Standards Institute*
BESS	*Battery Energy Storage System*
BMS	*Battery Management System*
CC	*Coulomb Counting*
CE	*Coulombic Efficiency*
CSA	*Canadian Standards Institute*
DST	*Dynamic Stress Test*
ECM	*Equivalent Circuit Model*
EKF	*Extended Kalman Filter*
EV	*Electric Vehicles*
FUDS	*Federal Urban Driving Schedule*
HPPC	*Hybrid Pulse Power Characterization*
IEC	*International Electrotechnical Commission*
KF	*Kalman Filter*
LCO	*Lithium cobalt oxide battery cell*
LFP	*Lithium iron phosphate battery cell*
LKF	*Linear Kalman Filter*
LMO	*Lithium manganese oxide battery cell*
NMC	*Lithium nickel manganese cobalt oxide battery cell*
OCV	*Open-Circuit Voltage*
PDE	*Partial Differential Equation*
PF	*Particle Filter*
PNGV	*Partnership for a New Generation of Vehicles*
RES	*Renewable Energy Source*
SoC	*State-of-Charge*
SoH	*State-of-Health*
UKF	*Unscented Kalman Filter*
UL	*Underwriters Laboratories*
USABC	*US Advanced Battery Consortium*
UT	*Unscented Transform*

List of Figures

List of Tables

Abstract

Modern developments in electric mobility and continuously merging microgrids with high penetration of renewable energy sources have surged the demand for battery energy storage systems as a viable solution for storing the energy. The growing trend of the battery energy storage application in the last decade has given rise to recent investigations into battery energy storage management which aims to improve battery energy storage performance and extend the battery lifetime by reducing operational stresses, such as overcharging, deep discharging and overheating.

Battery energy storage safe operation and management rely on precise observation of the battery states, such as State-of-Charge and State-of-Health. The mentioned states have to be estimated as it is not possible to measure them directly.

In the literature, different battery State-of-Charge estimation methods are implemented considering a specific battery cell technology and application. Consequently, the identification of an appropriate State-of-Charge estimation method able to work properly in different applications and operational constraints is a challenge. Moreover, the choice of the suitable State-of-Charge estimation method is further hindered by the existing trade-off between complexity and accuracy offered by each method.

To address the aforementioned challenges, the present thesis is mainly focusing on developing the most frequently used Model-based State-of-Charge estimation methods by modeling a lithium nickel manganese cobalt oxide (NMC) battery cell, which is one of the most successful lithium-ion battery cell technologies within the industry sector.

The Model-based estimation structures developed with three different equivalent circuit models and verified State-of-Charge estimators, are tested by applying dynamic and constant current profiles at different C-rates and operating temperatures. The results achieved through the tests are used for comparison and evaluation of Model-based structures to identify the accuracy of each algorithm, as well as their advantages and constraints concerning the possible applications.

Sommario

I moderni sviluppi nella mobilità elettrica e la continua evoluzione delle microreti con alte penetrazioni di fonti rinnovabili, stanno aumentando la domanda di sistemi di accumulo di energia elettrica. La crescita di queste applicazioni, nell'ultimo decennio ha portato a un grande sviluppo di soluzioni di accumulo a batterie elettrochimiche gestite da sistemi elettronici di conversione. Ciò ha dato origine a diversi studi associati alla gestione della carica delle batterie al fine di migliorarne le prestazioni e prolungarne la vita utile riducendone gli stress operativi (come sovraccarico carica/scarica e temperature operative eccessive).

Un funzionamento e una gestione sicura della batteria si basa quindi sull'osservazione dello stato della stessa, come lo stato di carica o lo stato di salute, che deve essere osservato con precisione. Va notato che qualunque sia lo stato della batteria di interesse, questo deve essere stimato in quanto non è possibile misurarlo direttamente.

Considerando lo stato di carica della batteria, nella letteratura sono disponibili diversi metodi sviluppati ed utilizzati in considerazione di una specifica tecnologia di batteria e applicazione. Di conseguenza, identificare un metodo appropriato di stima dello stato di carica di una particolare tecnologia di accumulo considerando applicazioni diverse è di per se una sfida. A complicare il problema è anche importante sottolineare che il compromesso esistente tra complessità e precisione è un ulteriore ostacolato alla scelta di un metodo di stima dello stato adeguato a più applicazioni.

Per affrontare le sfide di cui sopra, la presente tesi si concentra principalmente sullo sviluppo dei metodi di stima dello stato di carica basati sui modelli più frequentemente utilizzati, sviluppando una batteria al Litio Nichel-Manganese-Ossido di Cobalto (NMC), che è una delle batterie al litio di maggior successo tra le tecnologie delle celle a batteria agli ioni di Litio. Le strutture di stima dello stato di carica basate sul modello sono sviluppate considerando tre diversi modelli equivalenti di batteria e tre stimatori dello stato di carica. Ciascuna delle strutture di stima dello stato di carica è stata testata considerando profili di corrente dinamici e costanti (con tassi di C diversi) e temperature di esercizio differenti. I risultati ottenuti attraverso i test vengono utilizzati per confrontare e valutare le strutture di stima dello stato di carica basate su modello per identificare l'accuratezza di ciascun algoritmo di stima dello stato di carica della stessa batteria in diversi casi operativi.

Chapter 1

Introduction

This chapter represents the all-inclusive introduction to the present study and the fundamental concepts used in this thesis.

1.1 Context and Motivation

The lithium-ion battery cell technologies have proven their capability to store a significant amount of energy for a quiet long time. These criteria have promoted the lithium-ion Battery Energy Storage Systems (BESS) application in modern mobility (e.g. electric vehicles) and stationary (e.g. microgrids) solutions [1]. Consequently, many studies have analyzed the BESS from different perspectives, particularly trying to enhance BESS sizing, management, and performance concerning the application requirements.

One of the important factors frequently addressed in the literature is the battery State-of-Charge (SoC), which indicates the relative amount of energy stored in a battery cell, defined as the ratio of the available capacity of the battery cell to its nominal capacity. Accurate estimation of SOC not only ensures battery cell safe operation, prevents overcharging, avoids deep discharging, and improves the battery life, but also allow the application to make rational control strategies to save more energy.

The battery SoC cannot be measured, thus to determine its value, different estimations methods can be employed. These methods mainly use the realistic data collected from measurable variables of the battery cell, such as terminal voltage, current, and operating temperature to perform the state estimation.

The battery SoC can be estimated offline, for which the battery must be detached from the load or charging source. Although offline SoC estimation is only based on direct measurements and simple, it is time-consuming and not efficient due to the fact that the BESS operation is interrupted for a quiet long period of time required for the battery to reach a chemically stable point where accurate measurement can give precise SoC estimation [2]. Therefore, it can be concluded

that the offline method is mainly suitable for battery cell characterizing analysis by the manufacturers, and the modeling purposes.

Mentioned disadvantages and the requirements of the modern applications have raised interest in the Model-based SoC estimation methods, which are capable to perform online SoC estimation, and reach desirable accuracy with the cost of higher complexity. The latter has led to the enduring trade-off between the accuracy and the complexity of the existing SoC estimation methods. Thus, making the best trade-off is the main motivation for the present study that aims to evaluate and compare the Model-based SoC estimation algorithms with respect to accuracy, complexity, and applicability by providing a clear insight into the advantages and disadvantages of each algorithm.

This objective cannot be achieved by simply referring to the literature due to the fact that the SoC estimation methods are mostly evaluated considering a particular application (e.g. specific battery cell technology, C-rate, and operating conditions). Consequently, a comprehensive study is required to address the challenges associated with the recognition of the suitable SoC estimation method for the desired application.

1.2 Literature Review

Since 1980 that the first lithium-ion battery was created, different research studies have been investigated to provide more in-depth knowledge of the battery cell characteristics and performance. The majority of these studies tend to address the topics related to the application of different commercial lithium-ion battery cells, such as lithium cobalt oxide (LCO), lithium iron phosphate (LFP), lithium manganese oxide (LMO), and lithium nickel manganese cobalt oxide (NMC), which are widely used in Electric vehicles (EVs) and electrical grids where distributed generation is realized using Renewable Energy Sources (RES).

Studies [3–7] are based on comparing different Lithium-ion battery cell technologies by characterizing each cell based on specific power, specific energy, safety, lifespan, cycling at low/high C-rates, and thermal stability. The studies also include the manufacturing costs of lithium-ion batteries employed for different applications.

Mentioned studies agree that the lithium-ion batteries benefit from high energy density, low self-discharge rate, and require low maintenance. However, the manufacturers are constantly improving lithium-ion battery cell technologies in a way that new and more enhanced chemical combinations for battery cell development are introduced frequently. Therefore, more studies should be investigated to assess the advantages and disadvantages of each technology.

The comparative approach is similarly implemented in [8–11], which analyze the sizing and economics of different grid-connected lithium-ion BESS. These studies reveal that BESS sizing and technology are the key factors influencing the cost-efficiency of implementing energy storage systems due to high manufacturing costs of the lithium-ion battery cells. However, it is predicted that the lithium-ion battery cell price will be reduced due to recent technology improvements.

Although these studies incorporate valuable information that facilitate the recognition of suitable cell technology with respect to application, they are not addressing the BESS management and control.

Battery Management Systems (BMS) is responsible for managing the output, charging, and discharging the battery as well as preventing operational stresses. Practical analysis and design of BMS are the topics addressed in [12–15]. The authors have provided a comprehensive methodology to realize lithium-ion BESS management and control systems focusing on the conditions and requirements of a specific application. In these studies, the battery states such as SoC and State-of-Health (SoH) are considered among the factors that need to be observed by the BMS to implement the optimum control strategy. However, in these studies the state estimation procedure and methods are not analyzed thoroughly.

Accordingly, the battery state estimation methods are extensively studied during the recent decade trying to introduce a precise method that can fulfill the BMS requirements. Studies [16,17] propose different SoC estimation methods and provide an inclusive description of the proposed methods. On the other hand, the research works [18,19] are categorizing and comparing the different SoC estimation methods aiming to highlight the advantages and drawbacks of each method. The results verify robustness and accuracy of the Model-based SoC estimation methods.

For further analysis of the Model-based methods with respect to application conditions and constraints, the research studies [20–24] introduce different battery cell models and studies [25–32] include different SoC estimation algorithms that can be used to realize the Model-based SoC estimation structure.

The majority of the mentioned studies are using the modern control techniques and adaptive filtering methods to provide accurate SoC estimates, which are also compared in [33–35] considering a single battery cell model developed for a verified battery cell technology.

It is worth noting that, the Model-based SoC estimation is continuously improving by enhancing the battery cell models and introducing novel and hybrid estimation algorithms as in [36–41]. The new SoC estimation techniques tend to improve estimation accuracy by eliminating the flaws described for the other algorithms. However, some of these techniques are developed recently and further research is required to evaluate their performance with different battery cell technologies and conditions.

According to the literature review, numerous research works have implemented the Model-based method for the lithium-ion battery cell technologies. Although these studies represent successful approaches resulting in high SoC estimation accuracy, they are not including the evaluation of different battery cell models in integration with different SoC estimation algorithms for a unique battery cell technology. The latter is addressed in the present thesis, which provides more comprehensive and inclusive analysis of the most used Model-based SoC estimation methods.

1.3 Adopted Battery Cell technology

The battery cell technology adopted for the present study is known as NMC battery cell with a solution of lithium hexafluorophosphate (LiPF6) in a mixture of organic solvent ethylene carbonate and ethyl methyl carbonate as the electrolyte. The cathode chemistry is nickel manganese cobalt oxide and the anode is graphite.

NMC batteries are among the frequently used lithium-ion batteries in the industry, e-bikes, EVs, and medical devices due to their high specific power, capacity, and extended lifetime.

Cathode combination of nickel and manganese has enhanced NMC batteries with high specific energy and low internal resistance. Additionally, low amount of cobalt in the cathode combination has resulted in lower cost and a higher market share in comparison to other lithium-ion battery cell technologies. The NMC battery cells are characterized with the lowest self-heating rate among all lithium-ion technologies. This is the other highlighted feature that has improved their safe operation and performance.

The adopted battery cell nominal voltage is 3.6 V, and the nominal capacity is equal to 8 Ah. The cell is manufactured as a pouch cell with 16 layers and the size is equal to $105 \times 100 \times 7.05$ mm with weight equal to 157 g [42].

1.4 Model-Based SoC Estimation

Model-based SoC estimation methods are verified as robust and efficient techniques that can be implemented for online SoC estimation. The lithium-ion battery cell technologies are complex electrochemical systems with non-linear and time-variant characteristics. Therefore, for SoC estimation, the Model-based methods with a closed-loop structure can be the promising solution as they are able to improve the estimation by reducing the error. This property also makes the Model-based SoC estimation methods less dependant on the estimated initial SoC.

The Model-based SoC estimation structure is illustrated in Figure 1.1. As it can be seen, the Model-based SoC estimation structure consists of a battery model and the SoC estimation algorithms.

The model inputs are obtained through direct measurements of the battery charging/discharging current and temperature. The Coulomb Counting (CC) method is used for predicting primary SoC that is required by the battery model for parameter identification.

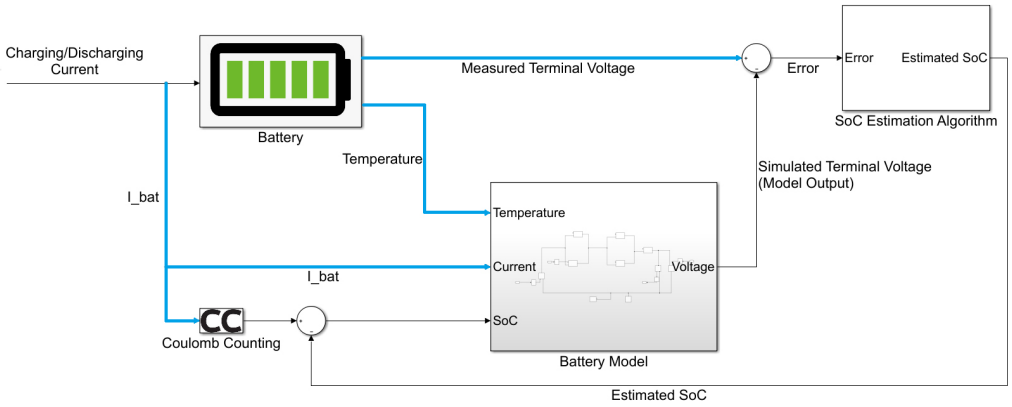

Figure 1.1: Model-Based SoC estimation structure.

The Model-based SoC estimation is based on the assumption that the battery model is equivalent to the real battery cell so that it can simulate the battery behavior with significant correspondence [21]. Therefore, considering identical inputs for both battery cell and the model, it is expected that the output voltage simulated by the battery model will be equal to the real battery terminal voltage. However, in real applications, the model and sensors, which are used to measure the input parameters, are non-ideal and noisy. The presence of the noise and inaccuracies in model development are the main sources of the SoC estimation error.

To reduce the error, the SoC estimator tends to calculate a system gain based on the deviation between battery model output and the actual battery cell terminal voltage. The calculated gain is efficiently used for correcting and improving the estimated SoC. However, it should be noted that the estimator gain is not used for correcting the modeling errors. Thus, the model accuracy has an inevitable effect on the SoC estimation obligating the precise battery modeling for achieving better results.

To reach trusted and precise estimation results, the battery model must be developed considering the cell electrochemical characteristics. Studies have shown that battery electromotive force, which is used to approximate the battery Open-Circuit Voltage (OCV), can be measured with respect to SoC variation.

The resulting OCV-SoC function, which is nonlinear monotone for NMC battery cells contains the fundamental information required for SoC estimation and BESS management [11,43]. Therefore, accurate OCV measurement is pivotal for battery modeling.

Precise OCV measurement is complex since the battery behavior is affected by its transient state, Hysteresis phenomena, charging and discharging rate (C-rate), and aging. Therefore, the impact of each factor must be analyzed and considered during the battery cell modeling process.

The electrochemical processes, such as diffusion and charge-transfer occurring at the interface between electrolyte and electrodes are responsible for the dynamic battery voltage transient, which is visualized in Figure 1.2 .

It can be seen that, there is an immediate voltage drop once the discharging current pulse with C-rate of 1C (8 A) is applied at $t = 2.21 \times 10^4$ s. This sudden voltage drop, which is indicated by ($\triangle V_1$), is caused by the internal resistance of the cell, and the resistance of active material, such as electrolyte and current collector.

During the discharging process at a constant 1C rate, the battery cell voltage shows an exponential decay ($\triangle V_2$), which is mainly caused by the surface reactions and the diffusion effects.

At $t = 2.245 \times 10^4$ s, as the discharging current pulse goes to zero, an immediate voltage rise ($\triangle V_3$) can be observed. The sudden voltage rise can be explained by pointing out that the effect of the cell internal resistance is removed when the battery current is equal to zero. However, the battery cell is still affected by the surface reactions and the diffusion effects that are shown by an exponential rise ($\triangle V_4$), which demonstrates that the OCV converges to the steady-state value gradually.

Accordingly, for modeling the battery cell precisely, the OCV value must be measured after the end of the charging/discharging sequence, and allowing the battery to reach steady-state considering adequate relaxation time.

The exponential decay and rise in the battery voltage transient state can be modeled considering specific time constants, which will be further discussed in Section 2.1. The relaxation time required for each battery cell varies according to cell technology and age.

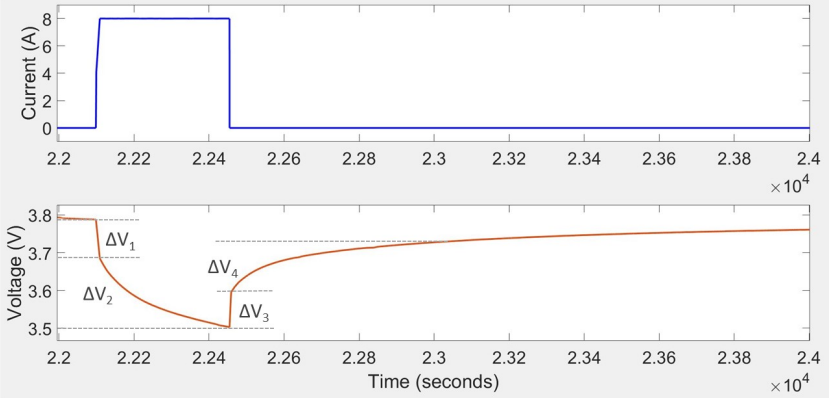

Figure 1.2: Battery cell transient state when a discharging current pulse with C-rate of 1C is applied.

By further analysis in battery cell, it has been observed that in real battery cells, the OCV measured at a certain SoC is not equal to a single and stable value and

its value varies within a specific range. This effect is described as **Hysteresis phenomena** [44].

The voltage hysteresis, which is time-independent and changes only with respect to SoC variation, has positive value during the charging process and negative value during the discharging process; leading to different charging/discharging efficiency.

In the modeling process, the effects of charging/discharging current rate and the temperature on battery cell capacity should be considered as well. The **effective capacity**, which indicates the amount of energy that can be extracted from the battery, is lower when the battery is discharged with high C-rate since there isn't enough time for completion of the electrochemical processes inside the battery cell [17].

The effect of the battery cell temperature on its effective capacity can be analyzed using a constant current discharge test. The test is conducted at 3C rate (24 A) at different temperatures equal to 288.15 K, 298.15 K, and 318.15 K. The test results are shown in Figure 1.3. More detailed description of the constant current discharge tests is given in Section 4.1.

The results show that the battery effective capacity is elevated when the operating temperature is higher. The higher operational temperature lowers the battery internal resistance and facilitates the electrochemical reactions within the battery cell. However, prolonged cycling at high temperatures will shorten the battery lifetime.

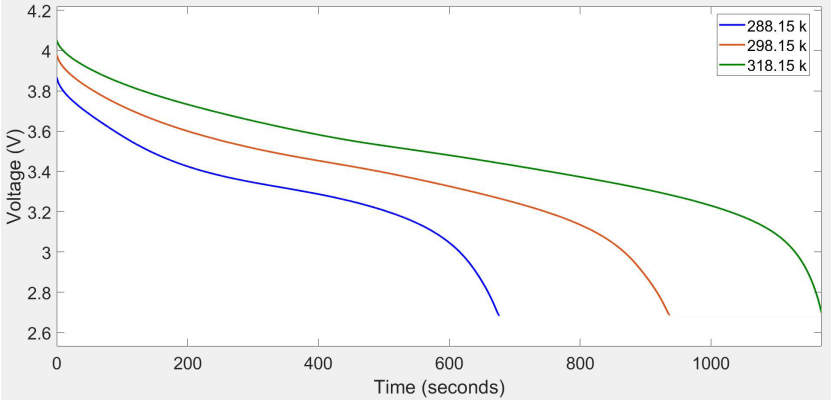

Figure 1.3: The battery cell effective capacity at the constant current discharge with C-rate of 3C at temperatures 288.15 K, 298.15 K, and 318.15 k.

Another factor that needs to be considered for battery cell modeling is aging. **Battery aging** increases the cell internal resistance and degrades the battery cell capacity through the time. It should be noted that aging is inevitable. However, avoiding battery high rate cycling not only increases the battery effective capacity, but also decelerates battery cell aging.

1.5 Structure of the Thesis

The thesis is organized as follows: The battery models adopted for this study and the model development procedure are described in Chapter 2.
Chapter 3 provides introduction to the SoC estimation algorithms and a detailed explanation of each algorithm working principle and simulation.
Battery testing profiles, conditions, and test execution process are described in Chapter 4.
Chapter 5, is used for representing the obtained results and discussing the observations.
Finally, Chapter 6 is devoted to the conclusion and future research work recommendation.

Chapter 2

Battery Modeling

Different battery cell models studied in the literature [45–47], can be categorized as:

- Electrochemical models;
- Empirical/Analytical models;
- Data-Driven models;
- Electrical models.

The listed models are capable to simulate the battery cell operation in some regards and comprise the important modeling factors described in Section 1.4. Each model provides specific pros and cons. Therefore, employing a suitable model must be based on the operational conditions, application constraints, and required accuracy.

Electrochemical models, are developed to describe the electrochemical processes inside the battery cell using the nonlinear Partial Differential Equations (PDEs) [22, 48]. The equations are able to simulate the battery dynamic behavior precisely. However, the high computational effort and model complexity are two major drawbacks of the Electrochemical models.

Empirical/Analytical models, which are also known as simplified Electrochemical models, are developed using the reduced-order PDEs considering only the essential nonlinear characteristics of the battery cell. Consequently, compared to the Electrochemical models, both the computational burden and model accuracy are decreased [45, 49].
One of the frequently used Empirical model is battery Impedance model which is developed using electrochemical impedance spectroscopy techniques [50].
In brief, attempting to reach higher accuracy using Electrochemical and Empirical models will lead to undesirable complexity.

Data-Driven models are developed using data mining methods and Artificial Intelligence (AI) tools to simulate the battery cell performance [51, 52].

The data used at the model training stage is of paramount importance since it has a direct impact on model accuracy. Ease of use is a distinct advantage of Data-Driven models as they consider the battery system as a black-box. However, to reach higher accuracy, these methods require extensive training data-set. So it is necessary to collect adequate data implying more time-consumption and requiring numerous battery tests under different operational conditions. Furthermore, The complexity of these models prevents wide usage of AI based SoC estimations, since the computation resources available at real-life applications, such as EVs, are not enough for executing the estimations.

Electrical models known as Equivalent Circuit Models (ECMs) simulate the battery cell properties using electrical circuit elements, which make battery cell performance more comprehensible [24]. ECMs are widely used for SoC estimation in electrical grids with high penetration of RES and electric mobility applications due to their simple structure and adequate accuracy.

ECMs require lower computational resources with respect to Electrochemical models and provide further flexibility in application. However, it should be noted that the circuit elements parameter identification, which is the fundamental stage of developing an ECM , can be intricate and time-consuming.

Furthermore, as the model parameters are optimized considering the laboratory-test conditions, operating ECMs in a different condition might reduce the model accuracy [2].

Several other approaches toward maximizing the model accuracy by combining different battery cell models (e.g. Electrochemical models and ECMs) have been made to build hybrid models which benefit from the advantages of every single model. However, resulting hybrid models suffer from high complexity and applicability issues. To be more straight forward, a list of advantages and disadvantages of each battery cell model is reported in Table 2.1.

Considering the features described for each battery model, the ECMs are the optimal choice for the present study since their performance has been qualified for real-time (online) Model-based SoC estimation methods according to the investigated research works in recent years [53–55].

Table 2.1: Brief comparison of different battery cell models

Cell Model	Advantages	Disadvantages	Recommended Application
Electrochemical Models	- High accuracy; - Correspondence to the real battery.	- Requiring high computational effort due to model complexity; - Requiring fundamental knowledge of the battery electrochemical properties.	- Battery designing; - Lifetime estimation.
Empirical Models	- Higher abstraction and computational efficiency.	- Not being able to model the battery with high fidelity.	- Battery designing; - Battery parametric analysis; - Lifetime estimation.
Data-Driven Models	- High accuracy; - Not requiring a fundamental knowledge of battery electrochemical properties.	- Developing an extensive training data-set is laborious.	- SoC estimation; - Real-time BESS management and control.
ECMs	- Desirable accuracy; - Applicationally flexible and easily implemented;	- Complex parameter identification procedure; - Not being able to extrapolate well under different operational conditions.	- Online SoC estimation; - Real-time BESS management and control.

Main principle of ECMs is to take battery current, operating temperature, and SoC as the system inputs and model dynamic terminal voltage of the battery cell as the output. Different ECMs existing in the literature can be categorized as:

- Linear (R_{int}) model;
- Thevenin-Based models;
- Partnership for a New Generation of Vehicles (PNGV) models;

Further description about the model characteristics and development are given in the following sections. For more information about the PNGV, readers can refer to [24].

2.1 Adopted Equivalent Circuit Models

Recalling the main purpose of the current study, Linear model and the Thevenin-based models are employed since they fulfill the balance between model complexity and accuracy required for online Model-based SoC estimation considering the NMC battery cell technology.

Linear model, also known as R_{int} model is developed considering the battery cell internal resistance. The Linear model circuit is shown in Figure 2.1. The ohmic resistance R_{int} indicates the battery energy loss in the form of heat energy, which increases the battery operating temperature through cycling.

The battery OCV is modeled by an ideal voltage source (V_{OC}) and V_T is used to indicate the model terminal (output) voltage.

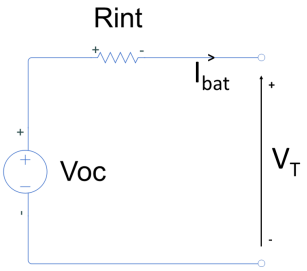

Figure 2.1: Linear model circuit diagram.

Although the Linear model is simple and easily applicable, it is not able to model battery transient response including diffusion voltage and the hysteresis phenomena.

The equation governing the Linear model is given as:

$$V_T = V_{OC} - R_{int} I_{bat} \tag{2.1}$$

Where I_{bat} represents the battery current.

According to (2.1), the model terminal voltage (V_T) is equal to the battery OCV when battery current is equal to zero($I_{bat} = 0$).

On the other hand, during charging/discharging process ($I_{bat} \neq 0$), the model is able to simulate the instantaneous change in voltage with respect to SoC variation. Consequently, this model is mostly employed for steady-state analysis and when the battery OCV-SoC function is approximately linear.

Thevenin-based models are the most frequently adopted ECMs for SoC estimation purposes [24].

These models are composed by adding resistor-capacitor networks (RC pairs) to the Linear model. The RC pairs are able to emulate the battery transient state including diffusion voltage and concentration polarization effects.

The Linear model with a single RC pair known as the **first-order Thevenin model** is shown in Figure 2.2.

The first-order Thevenin model benefits from one time constant ($\tau_1 = R_1 \times C_1$), to increase the model accuracy and fulfill the shortcomings of the Linear model.

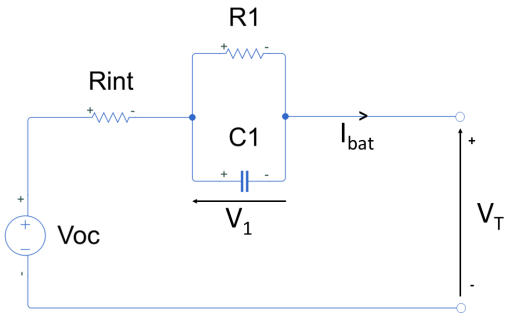

Figure 2.2: First-order Thevenin model circuit diagram.

The equations describing the first-order Thevenin model are given as:

$$\dot{V_1} = -\frac{1}{\tau_1}V_1 + \frac{1}{C_1}I_{bat} \tag{2.2}$$

$$V_T = V_{OC} - V_1 - R_{int}I_{bat} \tag{2.3}$$

Where $\dot{V_1}$ represents the derivative of the RC pair voltage (V_1) with respect to time.

It is possible to improve the model precision by connecting the second RC pair. The resulting model, known as the **second-order Thevenin model**, is represented in Figure 2.3.

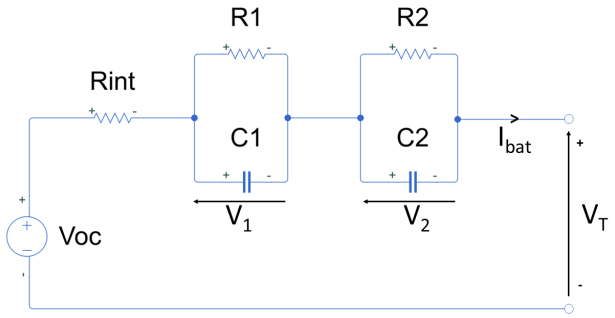

Figure 2.3: Second-order Thevenin model circuit diagram.

Studies present clear evidence that the second-order Thevenin models adopted for online SoC estimation, perform with desirable accuracy for certain battery cell technologies.

The model is enhanced with two different time constants ($\tau_1 = R_1 \times C_1$) and ($\tau_2 = R_2 \times C_2$) that facilitate the simulation of the short-term and long-term transient responses related to both electrochemical polarization and concentration polarization.

The equations describing the second-order Thevenin model are given as:

$$\dot{V_1} = -\frac{1}{\tau_1}V_1 + \frac{1}{C_1}I_{bat} \tag{2.4}$$

$$\dot{V_2} = -\frac{1}{\tau_2}V_2 + \frac{1}{C_2}I_{bat} \tag{2.5}$$

$$V_T = V_{OC} - V_1 - V_2 - R_{int}I_{bat} \tag{2.6}$$

It should be noted that adding the second RC pair has also increased model complexity. Thus, it is even possible to reach higher precision by adding more RC pairs if sufficient computational resources are available, and the application constraints, such as model complexity are not taken into account.

2.2 Model Development

The parameter identification process for ECMs is based on experimental data collected through the laboratory tests. Therefore, numerous tests at different conditions are required in order to develop an accurate battery cell model.

The model circuit elements (V_{OC}, R_{int}, R_1, C_1, R_2, and C_2) are not constant and vary with respect to the battery SoC and temperature [42]. Hence, to simulate the battery cell performance, each parameter should be identified.

In the present study, the battery self-discharge, which is usually modeled by ohmic resistance, is not considered due to the fact that it is relatively low for NMC and Lithium-ion battery technologies (2 - 3% per month). Moreover, the battery hysteresis phenomena, the SoH estimation, and battery aging analysis are out of the scope of present study. Consequently, the model parameters are developed as a function of SoC and operating temperature. The model performance is tested considering different C-rates and temperatures.

To identify each model parameter, a Hybrid Pulse Power Characterization (HPPC) test is intended by combining both charging and discharging current pulses to determine the battery power characterization profile. The HPPC test is performed with fully charged cell, and repeated at each 10% increment of SoC, until the cell got fully discharged. The pulse sequence included:

- Discharging the cell with current rate equal to 3C (24 A) for 10 s, followed by 180 s relaxation time;
- Charging the cell with current rate equal to 3C for 10 s, followed by 180 s relaxation time;
- Discharging the cell with current rate equal to 1C (8 A) until the SoC variation is equal to 10%, followed by 3600 s relaxation time;

The HPPC test current profile is shown in Figure 2.4. It should be noted that sufficient time must elapse until the battery reaches electrochemical equilibrium

before applying the next test current pulse. Considering relaxation time after every test sequence makes the testing process complicated and time-consuming.

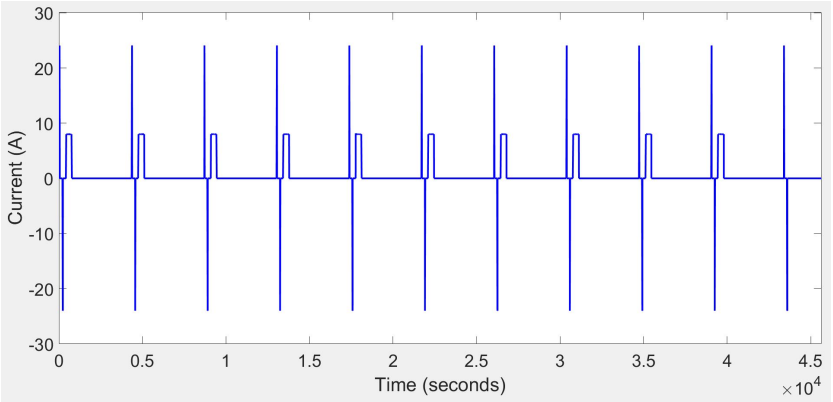

Figure 2.4: HPPC test profile.

2.3 Battery Cell Model Simulation

MATLAB Simulink® is used to model the ECMs adopted for this study. To build the ECMs, the related mathematical equations described in (2.1) - (2.6) are taken into account and for each of the model parameters (V_{OC}, R_{int}, R_1, C_1, R_2, and C_2), a lookup table is developed considering the break-point specifications equal to 0 to 100% with 10% increments for SoC and three different temperature rates equal to 288.15 K, 298.15 K, and 318.15 K. Cubic Spline algorithm is applied to identify the exact value of each model parameter according to the estimated SoC and measured temperature.

The lookup tables are connected to the corresponding variable electric elements as shown in Figure 2.5, which represents the Linear model.

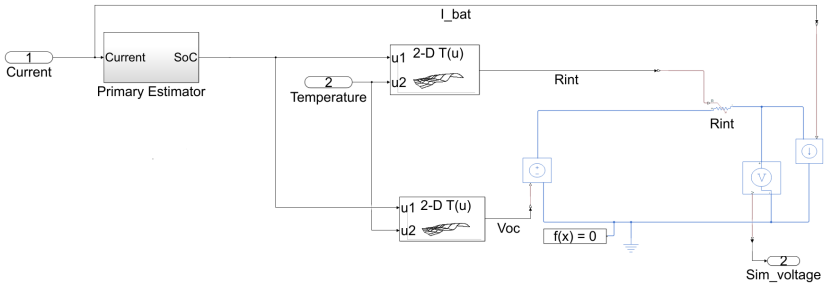

Figure 2.5: Simulated Linear ECM

The battery cell open-circuit voltage (V_{oc}) is simulated with a controlled voltage source. A controlled current source is hired to inject the battery cycling current

(I_{bat}), and an ideal voltage sensor, which converts the voltage measured between any electrical connections into a physical signal proportional to the voltage, is used to measure the simulated terminal voltage of the simulated ECMs.

Similar structures are developed to realize the first-order Thevenin model and the second-order Thevenin model, which are represented in Figure 2.6 and Figure 2.7, respectively.

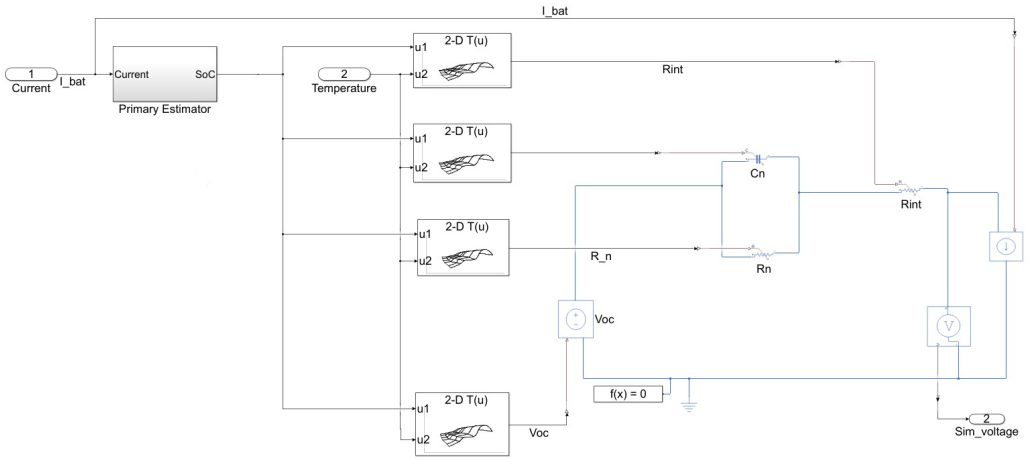

Figure 2.6: Simulated first-order Thevenin model.

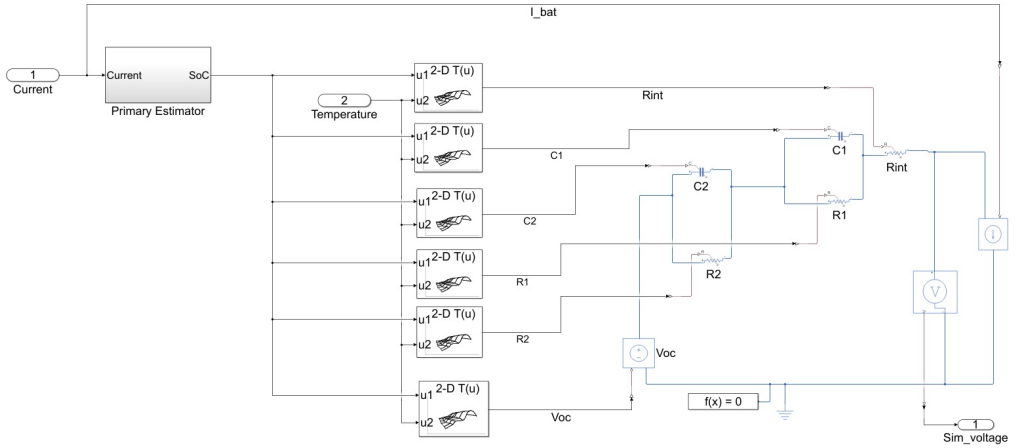

Figure 2.7: Simulated second-order Thevenin model.

The accuracy and performance of the developed models can be verified by comparing the simulated terminal voltage (V_T) and the battery terminal voltage measured through the HPPC tests. The comparisons are illustrated in Figure 2.8, Figure 2.9 and Figure 2.10, which represent the HPPC test result at 298.15 K (25° C) for each battery cell model.

It can be seen, that the models, which are developed independently, simulate the battery cell with acceptable accuracy and the model outputs are only slightly different.

The model validation with the HPPC tests at 288.15 K and 318.15 K are illustrated in Appendix A. The indications show that the models are capable to simulate the actual cell behaviour at different temperatures. The latter specify the compatibility of the developed models.

Furthermore, it is observed that the battery cell models developed using the data collected from the HPPC test at 318.15 K demonstrate higher accuracy. This can be explained by referring to the effect of the temperature on the actual battery cell performance. Higher operating temperature enhances the electrochemical processes inside the battery cell, reduces the battery internal resistance, and improves the battery cell's consistent performance.

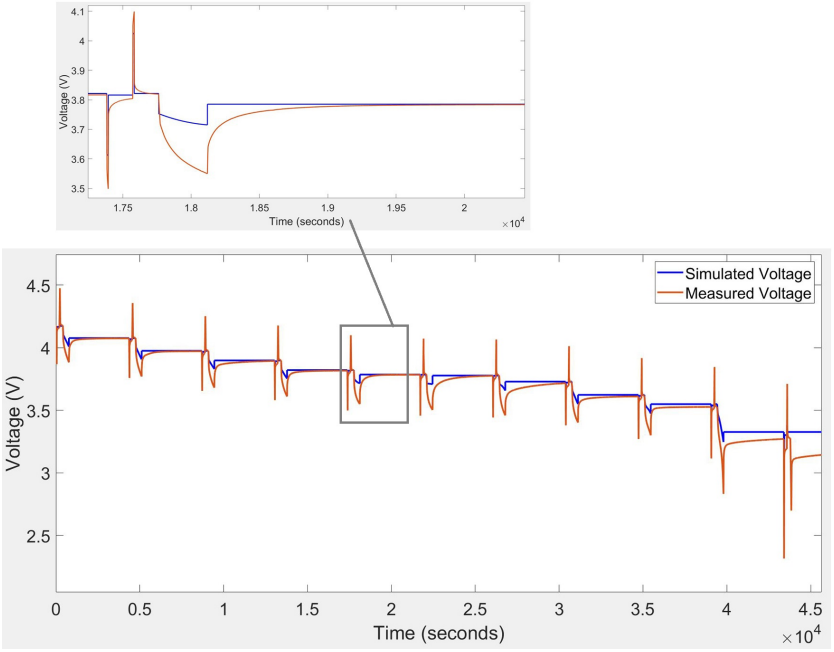

Figure 2.8: HPPC test voltage for Linear model at 298.15 K.

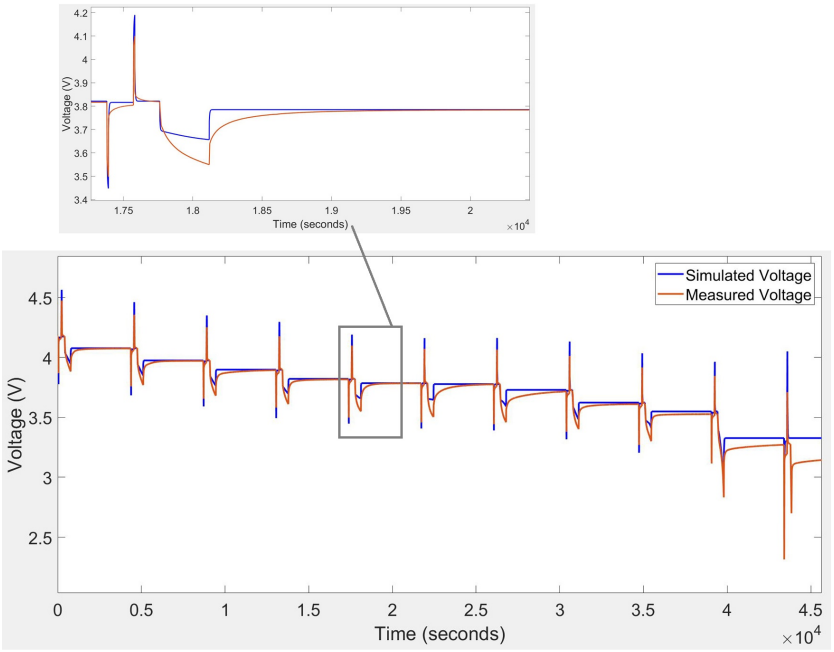

Figure 2.9: HPPC test voltage for first-order Thevenin model at 298.15 K.

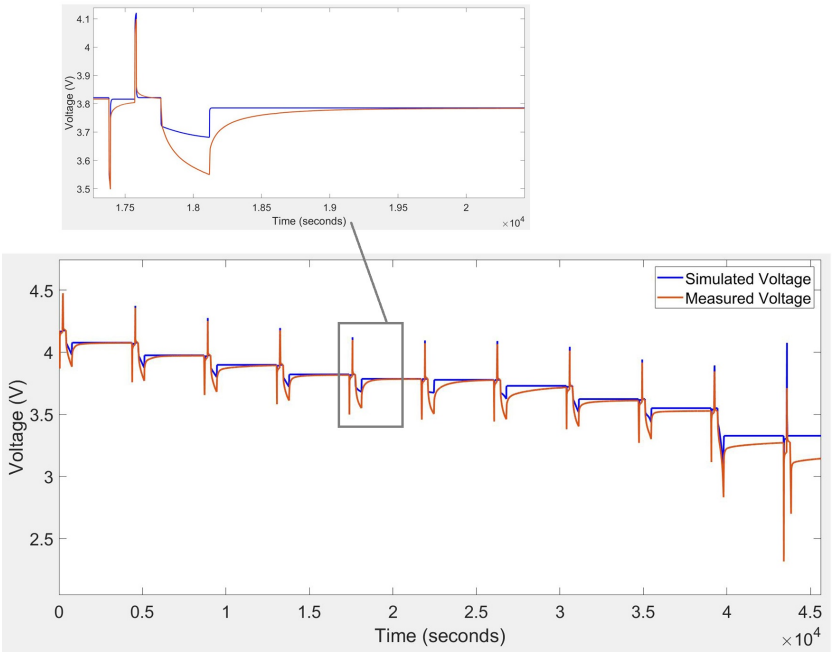

Figure 2.10: HPPC test voltage for second-order Thevenin model at 298.15 K.

Chapter 3

SoC Estimation Algorithms

Referring to Model-based SoC estimation described in section 1.4, it can be noticed that the Coulomb Counting (CC) method is responsible to provide primary SoC estimate required for model parameter identification. However, the CC is not the main SoC estimator since the Model-based SoC estimation methods are generally enhanced with more accurate SoC estimation algorithms.

Regarding the modern control theory, different adaptive filtering algorithms, such as Recursive Least Square, Particle Filter (PF), H infinity (H∞) filter, Kalman Filters (KFs), Luenberger observer, and the sliding mode observers could be employed to serve as the main SoC estimator [17, 56].

Numerous studies have applied the CC as the most common direct SoC estimation method and the KF algorithms as the efficient adaptive filtering methods. This is due to the fact that KF algorithms are computationally robust in comparison to the other suggested adaptive filtering algorithms.

The KF algorithms estimate an unknown system state variable based on the dynamic model of the system, system inputs, and the data collected by measuring the observable variables, which are considered to contain a certain level of uncertainty.

For the battery cell system, the uncertainties in battery current measurement can be considered as system process noise since they may alter the state of the system, and the voltage sensor inaccuracies can be modeled as the measurement noise because they are not affecting the system state directly. Taking these in mind, it can be concluded that KF can be an optimum solution as it can attain precise estimations by using self-correction mechanism when the measurements include statistical noise and sensor errors.

The KF algorithm assumes that all the system noises are Gaussian. Therefore, it is possible to derive state estimation by implementing the Gaussian sequential probabilistic inference solution.

Different KF algorithms with specific properties can be found in the literature [17]. However, considering the non-linear characteristics of the NMC battery cell, Ex-

tended Kalman Filter (EKF) and Unscented Kalman Filter (UKF) are adopted for the present study since the Linear Kalman Filter (LKF), generally known as Kalman filter, works properly when the system is linear.

Consequently, the following sections are devoted to the in-detail description of the CC, EKF, and UKF estimators, including the theoretical and operational concepts.

3.1 Coulomb Counting

CC method uses the charging/discharging current for SoC estimation. The method is based on integrating the active flowing current (I_{bat}) measured over the specific time interval to indicate the amount of charge the battery cell has lost or gained in Ampere-second.

The amount of charge drawn from or supplied to the battery cell during the charging or discharging process per unit cell nominal capacity (Q_{rated}) indicates the SoC variation in percentage. Summing this value with the predetermined SoC at (t_0), denoted as initial State-of-Charge (SoC_0), will result in the updated SoC estimate.

The CC equation is given by:

$$SoC(t) = SoC_0 - \int_{t_0}^{t} \frac{\eta I_{bat}(\tau)}{Q_{rated}} d\tau \tag{3.1}$$

Where η indicates the Coulombic Efficiency (CE) that models the losses during the charging/discharging process. CE is the ratio of the total charge extracted from the battery during discharge process to the total charge put into the battery during the charging process through a full battery cycle. It should be noted that in the present study, the current is considered positive for the discharging process and negative for charging in the present study.

The CC method is simply applicable and computationally efficient. However, there are several factors that affect the accuracy of the SoC estimations.

First, as it was described in Section 1.4, the battery cell capacity is affected by the C-rating and operating temperature, which means that considering the constant capacity (Q_{rated}) as reference would cause a non-negligible error.

Second, the inaccuracy in estimation of SoC_0 and approximation of η, may be the other source of the estimation error.

Finally, the current measurement is not ideal and the current flowing from/to the battery cell is different from what is measured due to the existing sensor error and measurement noise. Moreover, by using the CC method the self-discharging and leakage currents are usually neglected.

The mentioned factors are the main reasons for the integrated error and drift in the estimated SoC, which cannot be compensated since there is no feedback or correction mechanism. The latter confirms the necessity of using EKF or UKF as the main estimators for the Model-based SoC estimation.

3.2 Extended Kalman Filter

The EKF, which is the extended version of the standard LKF, is capable to execute state estimation in integration with the nonlinear systems.

The estimation procedure, which is based on the sequential probabilistic inference solution is valid for both LKF and EKF under the assumption that the noises are Gaussian. However, to cope with nonlinear systems, the EKF uses the linearization technique, analytically applied at each operating point. The linearization technique is computationally efficient when the system is not highly nonlinear [2].

To use EKF estimator, the battery cell system should be modeled using the discrete-time state-space equations given in (3.2) and (3.3).

$$x_k = f(x_{k-1}, u_{k-1}) + w_{k-1} \tag{3.2}$$

$$y_k = g(x_k, u_k) + v_k \tag{3.3}$$

Where x_k and y_k represent the system state vector and the system output measured at time step (k), respectively. The state transition function $f(x_{k-1}, u_{k-1})$ is defined based on the previous state and the measured system input (u) which are indicated by time index $(k-1)$ and the measurement function $g(x_k, u_k)$ is defined based on the current state of the system and the input at time step (k). The elements w_k and v_k depict the process and measurement noises, respectively.

Both w_k and v_k are considered additive and independent white Gaussian noises with zero mean and specified covariances equal to Q_w and R_v, respectively.

According to characteristics of the battery cell system employed for this study the functions $f(x_k, u_k)$ and $g(x_k, u_k)$ are non-linear and from the functional point of view, the state transition function $f(x_{k-1}, u_{k-1})$ is used to predict the current state of the system based on the previously estimated state and the measurement function $g(x_k, u_k)$ is used to predict system output based on the current state of the system.

The system state vector is defined based on the battery cell model. Therefore, for Linear model the state vector can be defined as:

$$x_k = \begin{bmatrix} SoC_k \end{bmatrix} \tag{3.4}$$

and for first-order Thevenin model it can be written as:

$$x_k = \begin{bmatrix} SoC_k \\ V_{1,k} \end{bmatrix} \tag{3.5}$$

Finally, for the second-order Thevenin model it is defined as:

$$x_k = \begin{bmatrix} SoC_k \\ V_{1,k} \\ V_{2,k} \end{bmatrix} \tag{3.6}$$

The system input (u_k) is equal to the battery current (I_{bat}) measured in discrete-

time with sampling time (T_s). The battery cell terminal voltage (V_T)is considered as the measured system output (y_k).

The EKF linearization technique, which tends to linearize system equations at every operating point, is realized by applying Taylor series expansion with the simplifying assumptions that the higher-order terms are negligible and the functions $f(x_k, u_k)$ and $g(x_k, u_k)$ are differentiable at every point in their domains. The stated simplifying assumptions are the main drawbacks restricting EKF application for highly non-linear systems.

By applying the first-order Tylor series expansion, (3.2) and (3.3) can be rewritten in the linear form, given as:

$$x_k = A_{k-1}x_{k-1} + B_{k-1}u_{k-1} + w_{k-1} \tag{3.7}$$

$$y_k = C_k x_k + D_k u_k + v_k \tag{3.8}$$

Where A_k, B_k, C_k, and D_k are the matrices analytically determined with partial derivatives (Jacobians) of the system functions $f(x_k, u_k)$ and $g(x_k, u_k)$ with respect to system state x_k and the measured input u_k as given in (3.9) - (3.12).

$$A_k = \left.\frac{\partial f(x_k, u_k)}{\partial x_k}\right|_{x_k=\hat{x}_k^+} \tag{3.9}$$

$$B_k = \left.\frac{\partial f(x_k, u_k)}{\partial w_k}\right|_{w_k=\overline{w}_k} \tag{3.10}$$

$$C_k = \left.\frac{\partial g(x_k, u_k)}{\partial x_k}\right|_{x_k=\hat{x}_k^-} \tag{3.11}$$

$$D_k = \left.\frac{\partial f(x_k, u_k)}{\partial v_k}\right|_{v_k=\overline{v}_k} \tag{3.12}$$

where the notation "^" indicates the estimated values and the notations "-" and "+" are denoting the prior and posterior estimates, respectively.

Considering system functions $f(x_k, u_k)$ and $g(x_k, u_k)$ and the state vectors defined for each model, the matrices A_k, B_k, C_k, and D_k will have different in dimensions and the elements for each battery cell model.

For second-order Thevenin model, the Jacobian matrices can be defined as:

$$A_k = \begin{bmatrix} 1 & 0 & 0 \\ 0 & e^{-\frac{T_s}{\tau_1}} & 0 \\ 0 & 0 & e^{-\frac{T_s}{\tau_2}} \end{bmatrix} \tag{3.13}$$

$$B_k = \begin{bmatrix} -\frac{\eta T_s}{Q_{rated}} \\ R_1(1 - e^{-\frac{T_s}{\tau_1}}) \\ R_2(1 - e^{-\frac{T_s}{\tau_2}}) \end{bmatrix} \tag{3.14}$$

$$C_k = \begin{bmatrix} \frac{\partial V_{oc}}{\partial SoC}\Big|_{SoC_k} \\ -1 \\ -1 \end{bmatrix} \tag{3.15}$$

$$D_k = \begin{bmatrix} -R_{int} \end{bmatrix} \tag{3.16}$$

For the first-order Thevenin model and linear model, the Jacobian matrices A_k, B_k,and C_k can be defined by reducing the order of the matrices by removing the elements in the corresponding rows and columns. The Jacobian matrix D_k is the same for all ECMs developed for this study.

Having stated these, the recursive approach implemented by EKF can be described. The recursive calculation is initialized with the best guess of the current state and its error covariance(P_0^+), given as:

$$\hat{x}_0^+ = \mathbb{E}\left[x_0\right] \tag{3.17}$$

$$P_0^+ = \mathbb{E}\left[(x_0 - x_0^+)(x_0 - x_0^+)^T\right] \tag{3.18}$$

The notation "T" indicates the matrix transpose.

The initialization step is followed by the six analytical steps denoted as prediction and correction, which begins by propagating the mean and covirance of the input system state through the linearized system functions, described as:

- *Step 1: State - estimation time update*
  In this step, the priory state ($\hat{x}_k^-$) is predicted based on the posterior estimated state ($\hat{x}_{k-1}^+$) and the measured input (u_{k-1}), given as:

  $$\hat{x}_k^- = A_{k-1}\hat{x}_{k-1}^+ + B_{k-1}u_{k-1} \tag{3.19}$$

  The posterior estimated state (x_{k-1}^+) is set equal to ($\hat{x}_0^+$) when the EKF recursive calculations are executed for the first time.

- *Step 2: Error covariance time update*
  In this step, the error covariance ($P_{\tilde{x},k}^-$), which indicates the uncertainty of the state estimation achieved in (3.19), is calculated based on the error covariance of the posterior state ($P_{\tilde{x},k-1}^+$) and the process noise covariance (Q_w).

  $$P_{\tilde{x},k}^- = A_{k-1}P_{\tilde{x},k-1}^+A_{k-1}^T + Q_w \tag{3.20}$$

The error covariance of the posterior state ($P^{+}_{\tilde{x},k-1}$) is set equal to (P^{+}_{0}) when the EKF recursive calculations are executed for the first time.

- *Step 3: System output prediction*
  In this step, the system output ($\hat{y}_k$) is predicted based on the prior state estimated in (3.19) and the updated measured input (u_k), given as:

$$\hat{y}_k = C_k \hat{x}^{-}_k + D_k u_k \tag{3.21}$$

- *Step 4: EKF gain matrix calculation*
  In this step, the EKF gain matrix (L_k) is calculated according to the error covariance achieved in (3.20) and the measurement noise covariance (R_v).

$$L_k = P^{-}_{\tilde{x},k} C^{T}_{k} \left[C_k P^{-}_{\tilde{x},k} C^{T}_{k} + R_v \right]^{-1} \tag{3.22}$$

- *Step 5: State estimate measurement update*
  In this step, the posterior state ($\hat{x}^{+}_k$) is estimated based on the prior estimated state, EKF gain matrix, and comparing the actual system output (y_k), obtained by direct measurement from the actual battery cell, with the predicted system output ($\hat{y}_k$).

$$\hat{x}^{+}_k = \hat{x}^{-}_k + L_k (y_k - \hat{y}_k) \tag{3.23}$$

  The estimation achieved in this step will be substituted with the initialization state ($\hat{x}^{+}_0$) used for the next recursive approach.

- *Step 6: Error covariance measurement update*
  In this step, the error covariance indicating the uncertainty of the estimates achieved in (3.23) is computed as:

$$P^{+}_{\tilde{x},k} = (I - L_k C_k) P^{-}_{\tilde{x},k} \tag{3.24}$$

  where (I) indicates the identity matrix.

  The error covariance calculated in this step will substitute (P^{+}_{0}) for the the next recursive approach. The error covariance computed in this step is expected to have lower value in comparison to the error covariance achieved in (3.20), since the EKF gain matrix is used to apply corrections to the previously estimated values and increase the estimation accuracy.

The recursive approach executed by EKF is illustrated in Figure 3.1 ,which provides better insight into what has been discussed in this section.

There are two drawbacks for the EKF estimation algorithm. First, according to the battery cell system, the actual value of the state vector is unknown and it is considered as a random variable with a Gaussian distribution. Therefore, propagating only a single point (Gaussian mean) through the non-linear system functions may not be enough for producing precise estimations.

Second, the linearization process that leads to the linear approximation of the system functions around the mean of the input Gaussian distribution may increase

the inaccuracy and affect the estimation results adversely, such that a probable error in system modeling or estimating the initial state might lead to diverging results [2, 17].

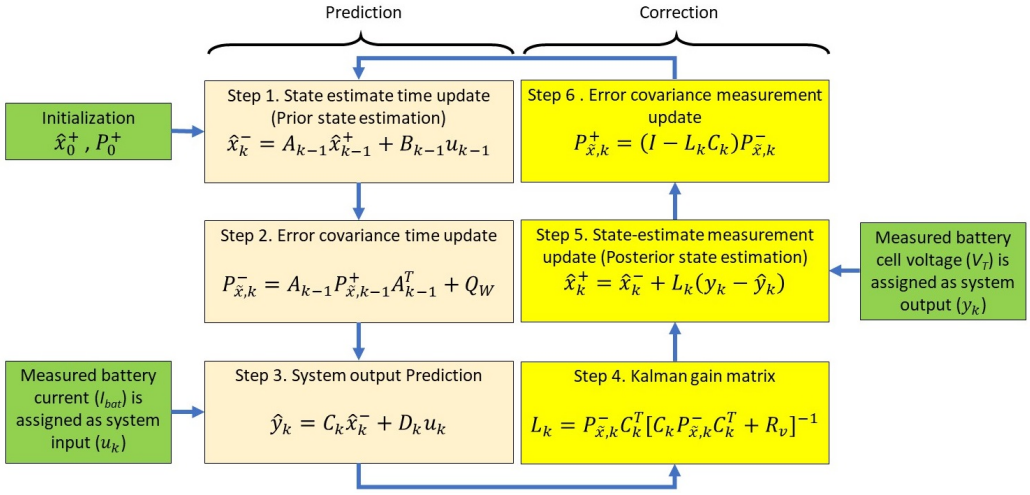

Figure 3.1: EKF recuresive state estimation flowchart.

For further information about the EKF estimation algorithm, it is recommended that readers refer to [2]

3.3 Unsented Kalman Filter

The UKF, which can be denoted as the updated version of the EKF, is the other frequently used state estimator that tends to improve estimations by addressing the drawbacks mentioned for the EKF. To do so, the UKF uses discrete-time filtering with Unscented Transform (UT) instead of the linearization technique.

To use UKF, the battery system should be modeled in a discrete-time, identical to what has been done in (3.2) and (3.3). The previously given information regarding the system state vectors, measured input and output, and the characteristics described for the process and measurement noises are also valid for the UKF.

The UKF working principle is to select a deterministic set of sampling points called sigma points on the Gaussian distribution of the system state vector. The selected sigma points are assigned weights in a way that the sum of the weights is equal to 1. Weighted sigma points are then propagated individually through the nonlinear system functions $f(x_k, u_k)$ and $g(x_k, u_k)$.

It is important to mention that propagating a random variable with Gaussian distribution through a nonlinear function will not result in a Gaussian distribution anymore. In this regard, the UT is responsible to approximate the Gaussian distribution of the transformed sigma points and to compute the corresponding mean and covariance.

The number of sigma points required by UT to approximate the output Gaussian distribution using the transformed sigma points, is equal to $(2n + 1)$ when the input mean and covariance are given in n-dimensions.

The first sigma point is the mean of the Gaussian and the others are symmetrically spread around the mean. The spread of sigma points is controlled by scaling factors denoted as Alpha (α), Kappa (κ), and Beta (β).

The spread is directly affected by the scaling factor Alpha and the square root of the scaling factor Kappa. Therefore, to control and limit the spread of the sigma points close to the mean, both Alpha and Kappa factors must be set to small values. The typical range for the scaling factors Alpha and Kappa are $10^{-3} \leq \alpha \leq 1$ and $0 \leq k \leq 3$, respectively [2, 57]. The scaling factor Beta, which incorporates the prior information of the state distribution, typically takes scalar values greater than zero. The optimal value of the scaling factor Beta for Gaussian state distribution is equal to $\beta = 2$. Assigning smaller values for the scaling factors will enable the UKF to easily track only a single peak in the probability distribution of the state. The latter possibly increases the precision of the state estimation.

Additionally, selecting the deterministic set of sigma points provides considerable advantages that distinguish UKF from EKF. Due to the fact that the linearization process is avoided, there will be no need to apply first-order Taylor series and computing the Jacobian matrices. Therefore, the system functions being differentiable at all operating points is no longer required, which means the UKF performance would be comparably better than EKF when the system under study is highly non-linear.

It is evident that using the set of points instead of one will relatively increase the complexity of the estimation algorithm. However, the UKF with a minimal set of sigma points would be computationally efficient in comparison to the PF algorithm which uses the higher number of randomly chosen points denoted as particles to simulate the input distribution.

It is necessary to go through a few important definitions before describing the UKF state estimation recursive calculation, which is also based on sequential probabilistic inference with six steps.

To implement UKF, a state vector (μ_k) should be defined to include the system state, the process noise, and the measurement noise at time index (k) as:

$$\mu_k = \begin{bmatrix} x_k \\ w_k \\ v_{k+1} \end{bmatrix} \tag{3.25}$$

which can be reported in the posterior estimation form, as:

$$\mu_{k-1}^{+} = \begin{bmatrix} \hat{x}_{k-1}^{+} \\ \overline{w} \\ \overline{v} \end{bmatrix} \tag{3.26}$$

including the mean values of all the random vectors with Gaussian distribution

affecting the system. The dimension of the state vector (μ^{+}_{k-1}) is used to define the number (n) which is used to identify the number of the sigma points required for the state estimation process. It will be recalled that the mean values for the process noise and the measurement noise are considered equal to zero.

The covariance matrix corresponding to the random state vector can be defined as:

$$P^{\mu,+}_{\tilde{x},k-1} = \begin{bmatrix} P^{+}_{\tilde{x},k-1} \\ Q_w \\ R_v \end{bmatrix} \tag{3.27}$$

The matrices defined in (3.26) and (3.27) are used to produce the sigma points, as:

$$\chi_{k-1} = \begin{bmatrix} \mu^{+}_{k-1} \\ \mu^{+}_{k-1} + \sqrt{(n+\lambda)P^{\mu,+}_{\tilde{x},k-1}} \\ \mu^{+}_{k-1} - \sqrt{(n+\lambda)P^{\mu,+}_{\tilde{x},k-1}} \end{bmatrix} \tag{3.28}$$

where (χ_{k-1}) is the matrix of the sigma points, chosen on the input state vector, and the scaling parameter (λ) is equal to:

$$\lambda = \alpha^2(n+\kappa) - n \tag{3.29}$$

After sigma points origination, it is possible to consider each row of its matrix as a separate section given as:

$$\chi_{k-1} = \begin{bmatrix} \chi^{x}_{k-1} \\ \chi^{w}_{k-1} \\ \chi^{v}_{k-1} \end{bmatrix} \tag{3.30}$$

Where (χ^{x}_{k-1}),(χ^{w}_{k-1}), and (χ^{v}_{k-1}) depict the randomness of the estimated state, the process noise, and the measurement noise, respectively.

It is now possible to represent the summarized UKF recursive approach, initialized with the best prediction of the system state and its covariance, given as:

$$\hat{x}^{+}_{0} = \mathbb{E}\left[x_0\right] \tag{3.31}$$

$$P^{+}_{\tilde{x},0} = \mathbb{E}\left[(x_0 - x^{+}_{0})(x_0 - x^{+}_{0})^T\right] \tag{3.32}$$

and followed by propagating the individual sigma points through the state transition function.

- *Step 1: State - estimation time update*
  In this step, the prior state of the system is estimated using the transformed sigma points and the measured input value, given as:

$$\chi^{x,-}_{k,i} = f(\chi^{x,+}_{k-1,i}, u_{k-1}, \chi^{w,+}_{k-1,i}) \tag{3.33}$$

$$\hat{x}_k^- = \sum_{i=0}^{2n} \gamma_i \chi_{k,i}^{x,-} \tag{3.34}$$

Where subscript (i) denotes the individual sigma point and the $(\chi_{k,i}^{x,-})$ depicts the matrix of the transformed sigma points. Finally, the prior state is estimated based on the weighted average of the transformed sigma points. This is done considering the weightening constant for mean computaions (γ_i) equal to:

$$\gamma_0 = \frac{\lambda}{n - \lambda} \tag{3.35}$$

$$\gamma_i = \frac{1}{2(n - \lambda)} \tag{3.36}$$

- *Step 2: Error covariance time update*
  In this step, the error covariance indicating the uncertainty of the prior state estimation is calculated based on the weighted sum of the results achieved for every sigma point (i) as:

$$P_{\tilde{x},k}^- = \sum_{i=0}^{2n} \rho_i (\chi_{k,i}^{x,-} - \hat{x}_k^-)(\chi_{k,i}^{x,-} - \hat{x}_k^-)^T \tag{3.37}$$

  where the weightening constant for covariance computaions (ρ_i) is equal to:

$$\rho_0 = \frac{\lambda}{n + \lambda} + (1 - \alpha^2 + \beta) \tag{3.38}$$

$$\rho_i = \frac{1}{2(n + \lambda)} \tag{3.39}$$

- *Step 3: System output prediction*
  In this step, the system output is estimated first, by propagating each of the transformed sigma points and updated input measurement through the system measurement function, and then calculating the weighted average, as:

$$Y_{k,i} = g(\chi_{k,i}^{x,-}, u_k, \chi_{k-1,i}^{v,+}) \tag{3.40}$$

$$\hat{y}_k = \sum_{i=0}^{2n} \gamma_i Y_{k,i} \tag{3.41}$$

  Where $(Y_{k,i})$ represents the matrix of individual sigma points propagated through the system measurement function.

- *Step 4: UKF gain matrix calculation*
  In this step, the UKF gain matrix (L_k) is calculated based on the covariance

matrices, given as:

$$P_{\tilde{y},k} = \sum_{i=0}^{2n} \rho_i (Y_{k,i} - \hat{y}_k)(Y_{k,i} - \hat{y}_k)^T \tag{3.42}$$

$$P^-_{\tilde{x}\tilde{y},k} = \sum_{i=0}^{2n} \rho_i (\chi^{x,-}_{k,i} - \hat{x}^-_k)(Y_{k,i} - \hat{y}_k)^T \tag{3.43}$$

Where arguments are previously calculated in steps 1 to 3. Therefore, the UKF gain matrix will be:

$$L_k = P^-_{\tilde{x}\tilde{y},k} P^{-1}_{\tilde{y},k} \tag{3.44}$$

- *Step 5: State estimate measurement update*
  Similar to step 5 of the EKF recursive approach, in this step, the posterior state ($\hat{x}^+_k$) is estimated based on the prior state, EKF gain matrix, and comparing the measured system output (y_k) and the predicted system output ($\hat{y}_k$), given as:

$$\hat{x}^+_k = \hat{x}^-_k + L_k(y_k - \hat{y}_k) \tag{3.45}$$

- *Step 6: Error covariance measurement update*
  The final step is also driven by computing the error covariance which indicates the error bound and uncertainty of the posterior state estimated in step 5, as:

$$P^+_{\tilde{x},k} = P^-_{\tilde{x},k} - L_k P_{\tilde{y},k} L^T_k \tag{3.46}$$

The estimation achieved in steps 5 and the error covariance calculated at step 6 will be substituted for the initialization parameters in the next recursive approach.

The UKF recursive calculations are visualized in Figure 3.2, in order to provide better insight into what has explained in the aforementioned steps. For further information about the UKF estimation algorithm, it is recommended that readers refer to [2, 17, 31, 58, 59]

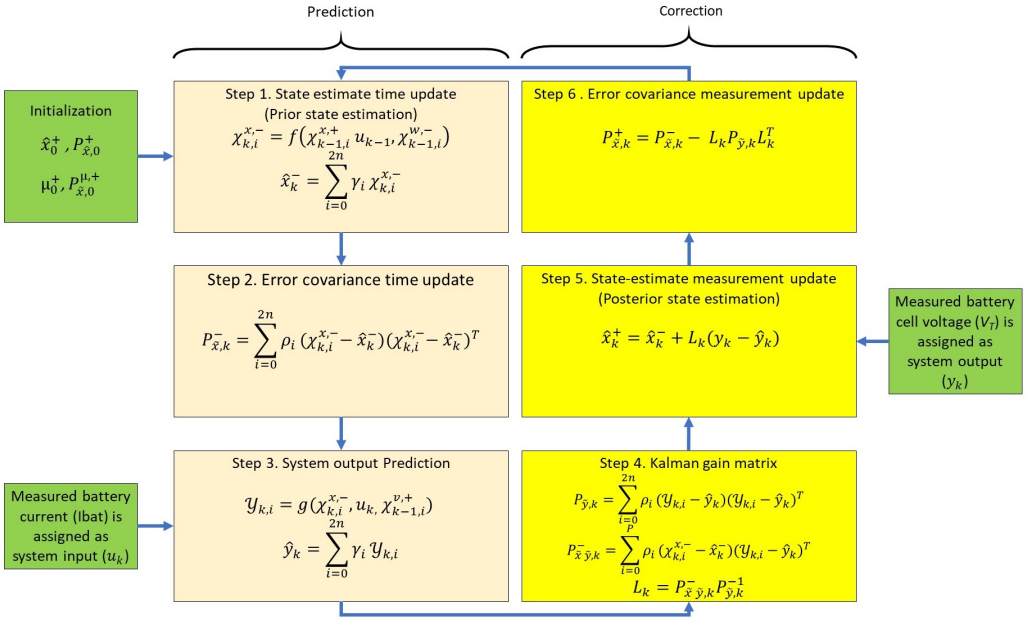

Figure 3.2: UKF recursive state estimation flowchart.

3.4 Estimator Simulation

To realize the Model-based SoC estimation structure, it is necessary to understand how to build and implement each block to enhance the integrated performance of the simulated system.

As described earlier, the CC algorithm is employed as the primary SoC estimator. To realize the CC in practice, the discrete-time summation is implemented instead of continuous integration to enhance the SoC updating process in each time step. The equation of the discrete-time CC algorithm is given in (3.47).

$$SoC_k = SoC_{k-1} - \frac{T_s}{Q_{rated}} \sum_{j=0}^{k-1} \eta I_{bat,j} \tag{3.47}$$

Where T_s represents the sampling time and the subscript (k) denotes the time index.

The simulated CC algorithm is shown in Figure 3.3. As it can be noted, the battery cell nominal capacity (Q_{rated}), which is typically reported in Ampere-hour, should be converted to the Ampere-second based on the sampling time chosen for the model operation. A unit delay block is used for sampling the battery current. A memory block is inserted to save the current SoC required as (SoC_{k-1}) for the next time step. The CE (η) is multiplied to the battery current, which is realized

with a gain block. Finally, a saturation block is used in the output to limit the SoC range between 0 - 100%.

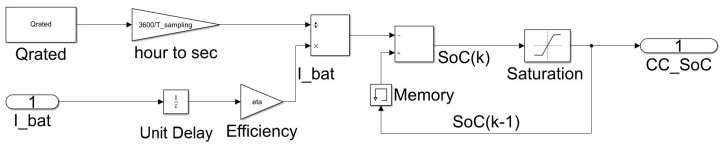

Figure 3.3: Simulated CC algorithm.

To implement the EKF and UKF in simulations, first, the system state transition and measurement functions are developed using Simulink function blocks [23]. The developed functions are later used within the EKF and UKF blocks that are implemented using MATLAB control system toolbox.

To perform the state estimation, the system functions are not the only parameters required by EKF and UKF estimators. The process noise covariance, measurement noise covariance, the initial state of the system, the initial error covariance, and the scaling factors α, κ and β are the other parameters that should be set as well. The mentioned parameters will be briefly denoted as the **tuning parameters** of the EKF and UKF estimators. In the present study, EKF and UKF tuning parameters, and the test conditions are defined in a way to be inclusive and to provide a meaningful and precise comparison of the Model-based SoC estimation algorithms. The applied conditions and parameters can be summarized as:

- To simulate measurement noise two independent noise with power equal to 1×10^{-3} and 1.5×10^{-3} are considered to be added to the input current and the model output voltage, respectively.
- Each test is initialized with specific (SoC_0) described in Chapter 4. The initialization states defined for both EKF and UKF estimators according to each model are given in (3.48) - (3.50) for second-order Thevenin model, first-order Thevenin model, and Linear model, respectively.

$$\hat{x}_0^+ = \begin{bmatrix} SoC_0 & 0 & 0 \end{bmatrix} \tag{3.48}$$

$$\hat{x}_0^+ = \begin{bmatrix} SoC_0 & 0 \end{bmatrix} \tag{3.49}$$

$$\hat{x}_0^+ = \begin{bmatrix} SoC_0 \end{bmatrix} \tag{3.50}$$

  To define the initialization states, it has been considered that the battery cell is allowed to reach the chemical equilibrium through adequate relaxation time. The initialization values corresponding to RC pair voltages are set to zero as the battery current is considered equal to zero at t_0.

- The initial error covariance defined for both EKF and UKF estimators regarding the second-order Thevenin model, is given as:

$$P_0^+ = \begin{bmatrix} 10^{-3} & 10^{-1} & 10^{-1} \end{bmatrix} \times I_3 \tag{3.51}$$

where I_3 represents the identity matrix of order 3. Accordingly, for the first-order Thevenin model, it can be written as:

$$P_0^+ = \begin{bmatrix} 10^{-3} & 10^{-1} \end{bmatrix} \times I_2 \tag{3.52}$$

where I_2 represents the identity matrix of order 2. Finally, for Linear model it can be written as:

$$P_0^+ = \begin{bmatrix} 10^{-3} \end{bmatrix} \tag{3.53}$$

The initial error covariance matrices should be defined based on the initialization error. Therefore, if it is assumed that the predicted initial states are accurate and trusted, it is possible to assign lower values for the error matrices. Accordingly, in case the accuracy of the initial states are not assured, higher values should be assigned for the error covariance matrices.

- The process noise covariance defined for both EKF and UKF estimators considering the battery cell models are given in (3.54) - (3.56) for second-order Thevenin model, first-order Thevenin model, and Linear model, respectively.

$$Q_w = \begin{bmatrix} 10^{-8} & 10^{-6} & 10^{-6} \end{bmatrix} \times I_3 \tag{3.54}$$

$$Q_w = \begin{bmatrix} 10^{-8} & 10^{-6} \end{bmatrix} \times I_2 \tag{3.55}$$

$$Q_w = \begin{bmatrix} 10^{-8} \end{bmatrix} \tag{3.56}$$

The process noise covariance matrix indicates the amount of variance and covariance of the system states. The diagonal elements of Q show the variance of each state variable, and off-diagonal elements demonstrate the covariances between the different state variables. In this study, the covariance of the system state variables is considered zero since they are uncorrelated, and their variances, which are obtained empirically, are set to lower values indicating that the spread of the state variables is close to the mean of the distribution.

- The measurement noise covariance defined for both EKF and UKF estimators considering the battery cell models is given in (3.57), which is identical for all the models.

$$R_v = \begin{bmatrix} 10^{-2} \end{bmatrix} \tag{3.57}$$

In this study, the measurement noise covariance matrix contains only the variance of measurement related to the battery cell terminal voltage. The value is defined considering that the standard deviation of the measurement is equal to ($S = 0.1$) which indicates that measurement value spread is close to the mean of the Gaussian distribution.

- The UKF scaling factors are defined empirically as $\alpha = 10^{-2}$, $\kappa = 0$, and $\beta = 2$ to increase the accuracy of the UKF estimator.

- The sampling time defined for both of the estimator and the measurements is considered equal to ($T_S = 0.1$ s).

Chapter 4

Battery Testing Profiles

Battery testing is one of the most fundamental procedures that can be conducted to serve different purposes, such as qualification testing, safety and abuse testing, and performance testing.

The **qualifications testing** is designed to confirm the specifications introduced by the battery cell manufacturers and to verify whether the battery cell fits the desired operating conditions and requirements. The qualification testing includes the battery dynamic mechanical and environmental tests as well as the battery charging system tests to ensure that both systems are compatible and the battery cell will not experience irreversible overcharging stresses.

Safety and abuse testing are designed to verify that the battery cell is not a danger for the user or to itself under expected or worst-case accidental or deliberate abuse. Conditions to be investigated include vehicle crashes, exposure to external environments, and electrical charger malfunctioning. The data collected from these testings are used to ensure that the battery cell complies with the safety requirements and standards defined by national and international organizations.

Underwriters Laboratories (UL), American National Standards Institute (ANSI), Canadian Standards Association (CSA), and International Electrotechnical Commission (IEC) are among the organizations that have published standards concerning battery cell qualification, safety, and performance.

The **performance testing** is designed to verify whether the battery cell is able to deliver its specified power when needed. The performance testing includes the constant current discharge tests and constant, variable, and special power discharge tests that are all conducted considering the battery cell application and charging/discharging traits [60].

Battery cells and testing conditions are affected by various factors which may lead to deceiving results that possibly allow battery cells to mask the operational deficiencies. Therefore, the test conditions must be specified in a way that repeatable and meaningful results can be obtained.

Battery cell manufacturers are liable for their own end products. In this regard, they are responsible to conduct different tests to certify that the produced battery cells comply with the standards. However, the testing results achieved by the manufacturers only reflect the new battery specifications which do not consider battery aging and fading effects caused through the real-life application. The latter explains the reason why performance testing is of high importance.

The present study considers the performance testing conditions simulating the electric mobility and stationary applications, to compare and evaluate the online Model-based SoC estimation accuracy. For test execution, the battery cell CE is considered equal to ($\eta = 97\%$), and the sampling time is set to ($T_s = 0.1$ s).

To be more inclusive each test is repeated at four different temperatures equal to 288.15 k, 298.15 k, 308.15 k, and 318.15 K considering the typical battery operational temperature range in real-life applications. The extensive description of each test purpose and conditions are given in the following subsections.

4.1 Constant Current Discharge Test

Constant current discharge tests are performance testing types that are conducted with a sequence of discharging pulses at constant C-rate to evaluate the effective capacity of the battery cell.

In this study, a constant current with C-rate equal to 3C (24 A) is applied to the fully charged battery cell ($SoC_0 = 100\%$) to discharge the battery continuously without considering any relaxation time.

The 3C rate is denoted as the fast cycling C-rate that assumes that the battery cell will be required to deliver 24 A for 20-minutes. However, as a high discharge rate reduces the battery effective capacity, at 3C rate, the battery cell reaches the minimum discharge voltage corresponding to ($SoC = 0\%$), faster. The constant current discharge test profile is shown in Figure 4.1.

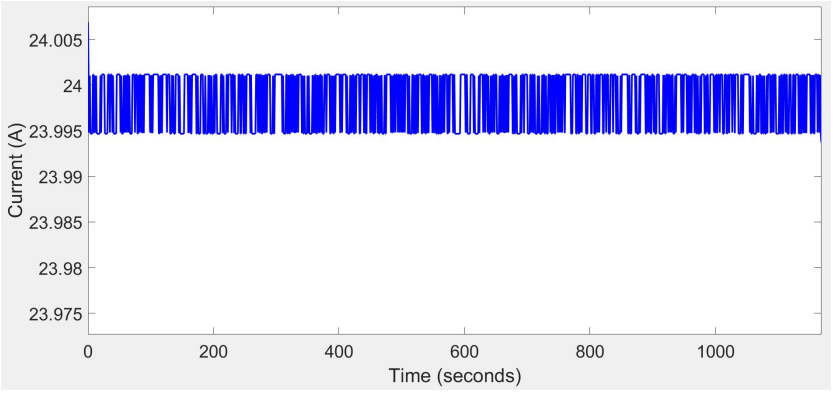

Figure 4.1: Constant current discharge test profile at 3C rate.

4.2 Federal Urban Driving Schedule Test

Federal Urban Driving Schedule (FUDS) is a standard variable power discharge test which is designed by US Advanced Battery Consortium (USABC) testing procedures.

The FUDS regime aims to simulate the effects of EV driving (including regenerative braking) on the performance of the battery cell. The regime is originally designed based on a complex 1372 s time-velocity profile collected from a specific vehicle driving data and then converted to the dynamic power-time profile [60].

To use the FUDS regime, the battery cell with ($SoC_0 = 80\%$) is charged with constant C-rate of 0.5C until the battery cell is fully charged. After 8543 s relaxation period elapsed, the battery cell is discharged with the same C-rate until the battery cell SoC drops to 80%. Considering enough relaxation time, the FUDS profiles are applied continuously end-to-end with no relaxation time between them, starting from $t = 18954$ s until the battery cell is fully discharged. The total test duration is equal to 3.068×10^4 s.

FUDS test profile is represented in Figure 4.2.

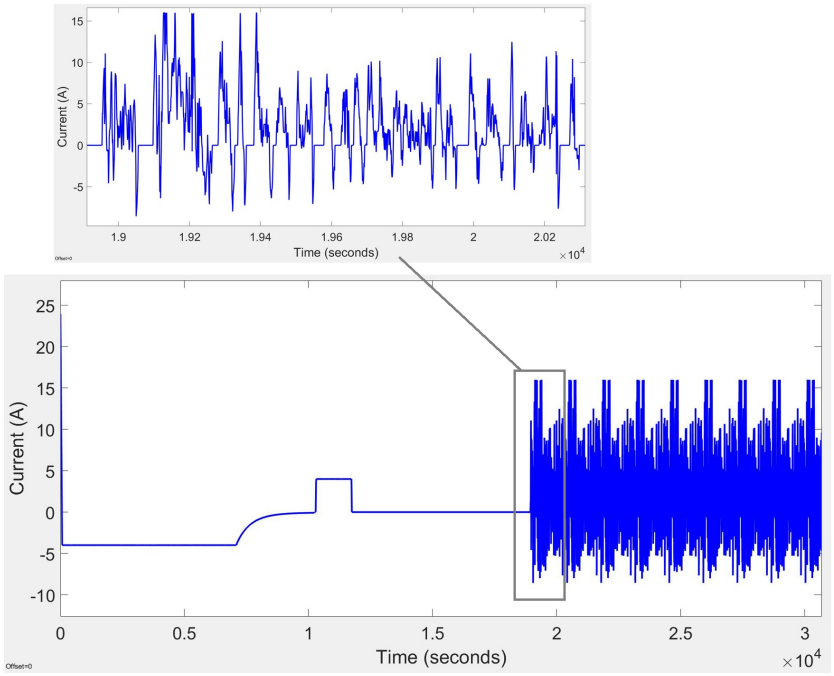

Figure 4.2: FUDS test profile.

4.3 Dynamic Stress Test

Dynamic Stress Test (DST) is the other variable power discharge regime that tends to simulate the discharging profile based on the data collected from driving a real

vehicle. The test is designed by USABC with a dynamic 360 s profile including regenerative breaking [60, 61].

To use the DST regime, first, the battery cell is fully charged with constant C-rate of 0.5C, followed by 1.42×10^4 s relaxation period. Then the battery cell is discharged with the same C-rate until the battery cell SoC drops to 80%. Relaxation period of 0.42×10^4 s is considered at this stage. Finally, the DST profiles are applied end-to-end repeatedly with no relaxation time between them, starting from $t = 2.30 \times 10^4$ s until the battery cell reaches the minimum discharge voltage.

The DST test profile is represented in Figure 4.3. The test is initialized with $SoC_0 = 60\%$. The total test duration is equal to 3.44×10^4 s.

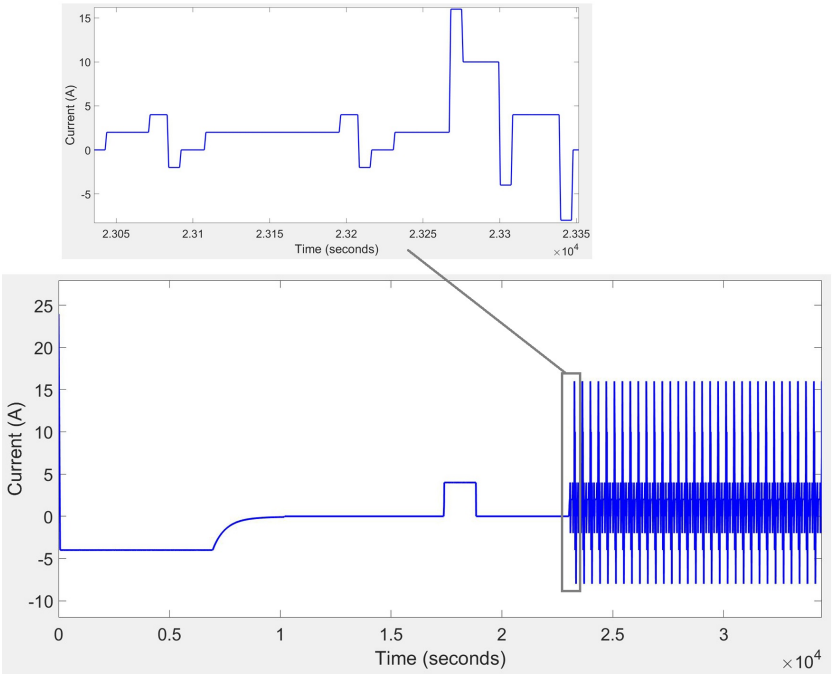

Figure 4.3: DST test profile.

4.4 Constant Current Cycling Test

Constant Current cycling test is designed to evaluate both the battery cell model performance and the SoC estimator accuracy when the battery is continuously cycled with the specific current rate in the SoC range between 20 - 70% .

The test profile that is represented in Figure 4.4 includes the sequence of discharging current pulses at C-rate of 1C applied for 1432 s, each followed by 125 s relaxation time and a charging pulse at 0.5C rate for 1730 s. The test starts with an initial SoC_0 equal to 50%. Then the battery is charged up to $SoC = 72\%$ and discharged to $SoC = 32\%$. The cycling profile is applied repeatedly, afterwards.

According to the test profile, the cycling proceeds for 2.85×10^5 s.

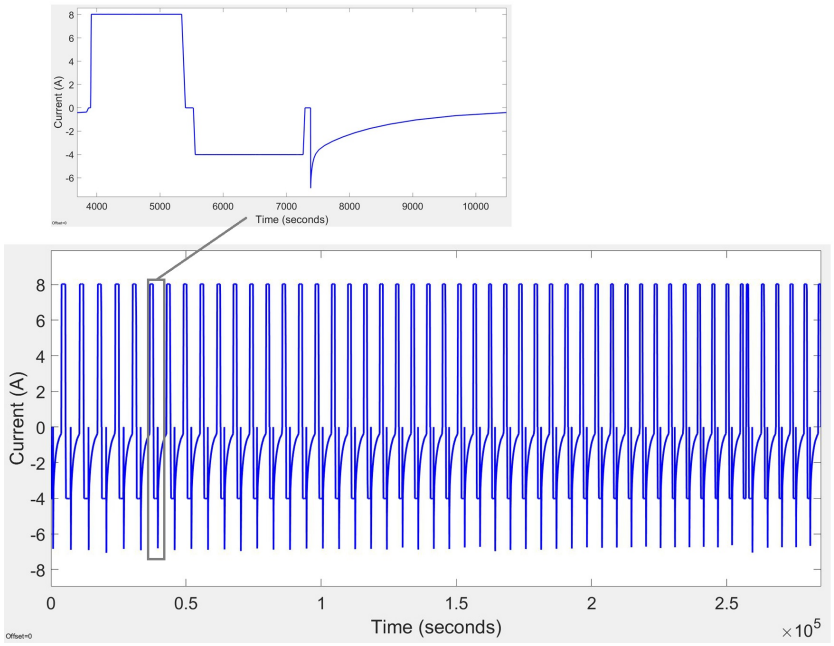

Figure 4.4: Constant current cycling test profile

4.5 High Regime Cycling

The High regime cycling test is designed to evaluate the battery cell model performance and the SoC estimator accuracy when the battery cell is cycled with a low current C-rate of 0.2C in a high regime partial charge/discharge cycle which means the battery cell cycled as the it consistently contains 70% of it nominal capacity available.

The test profile is given in Figure 4.5, which represents that the test is initialized with $SoC_0 = 70\%$ and the battery cell is discharged and charged once within the SoC range equal to 78 - 45%. Then the High regime cycling regime is applied continuously.

The expected SoC variation at each cycle is equal to 10% and the total test duration is equal to 4.91×10^5 s.

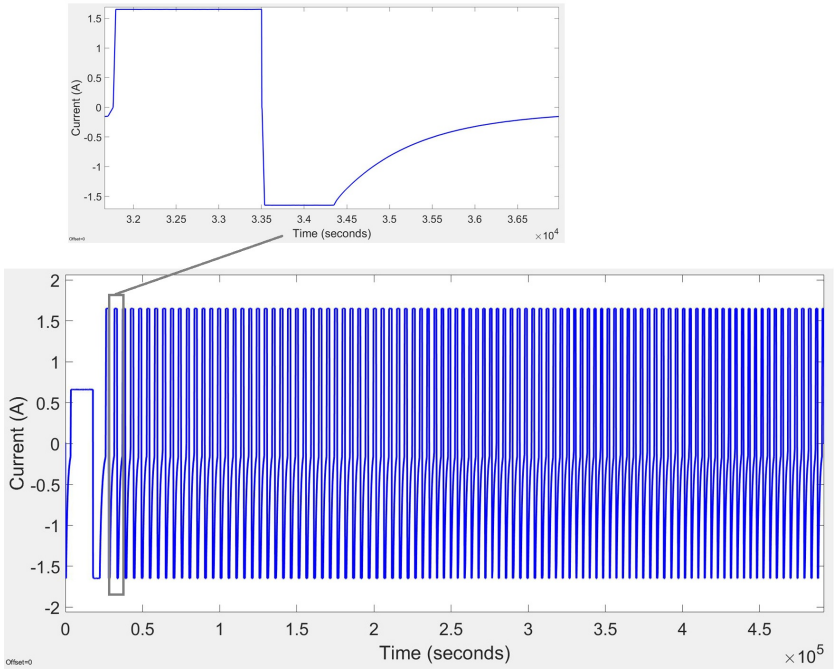

Figure 4.5: High regime test profile.

4.6 Low Regime Cycling

The low regime cycling test is similar to the High regime cycling test. However, this test tends to evaluate the model-based SoC estimation precision by cycling the battery cell at a 0.2C rate in a low regime partial charge/discharge cycle as the battery cell charge is always kept below 30%.

The Low Regime test profile is shown in Figure 4.6. The test is initialized with $SoC_0 = 20\%$ and the battery cell is charged and discharged once up to 57% and then, the low regime cycling profile is applied repeatedly. The expected SoC variation at each cycle is equal to 10% and the total test duration is equal to 4.88×10^5 s.

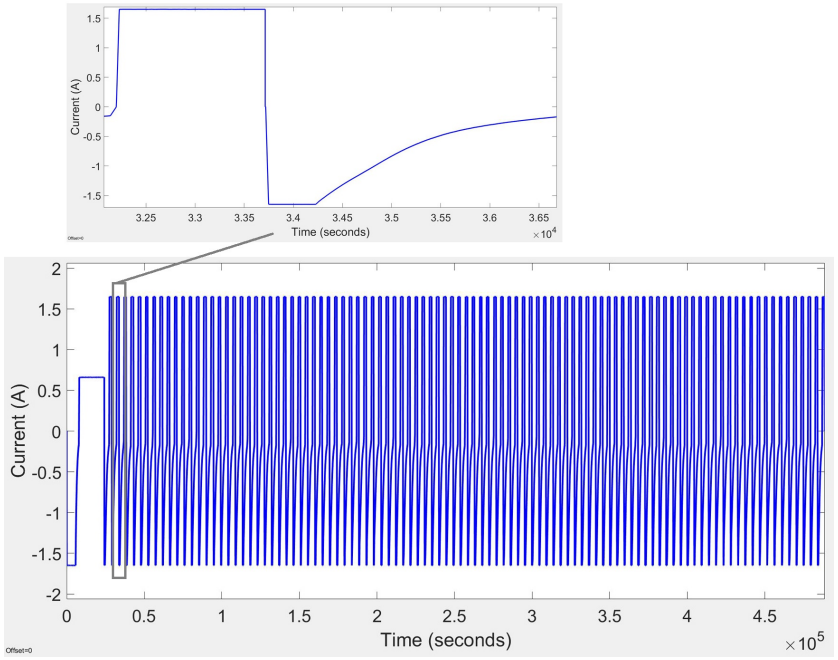

Figure 4.6: Low regime test profile.

Chapter 5

Results And Discussions

In this chapter, the SoC estimation results and the estimation error obtained from different tests are represented. The tests include HPPC, FUDS, DST, Constant current cycling, High regime cycling, and Low regime cycling profiles. The results are sorted with respect to the corresponding battery cell model in the following sections. To be able to demonstrate the SoC estimation error and compare the results from the precision point of view, a **Reference SoC** is considered which is obtained by the ideal integration of the battery cell current. To do so, the current measurement sensor error and noise are considered to be zero and the battery cell CE is set to 100%.

5.1 Results for Linear Model

The test results for running six different tests on the Model-based SoC estimation equipped with the Linear model are reported at a temperature equal to 298.15 k (25° C) in Figure 5.1 - Figure 5.12, which include the SoC estimation results and the corresponding estimation error.

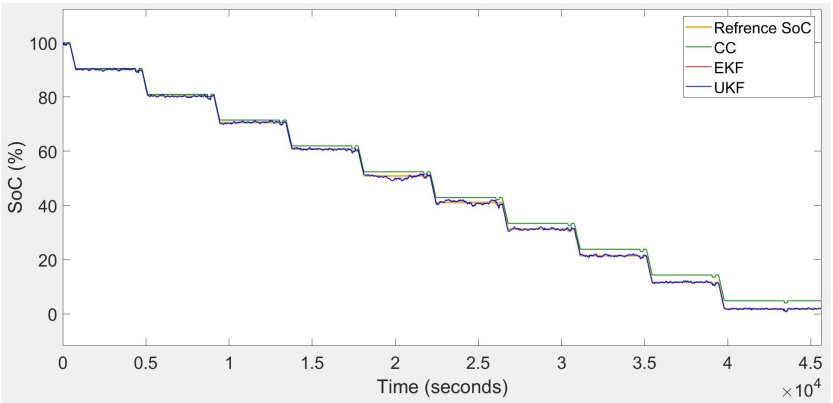

Figure 5.1: HPPC test - SoC estimation for Linear model at 298.15 K.

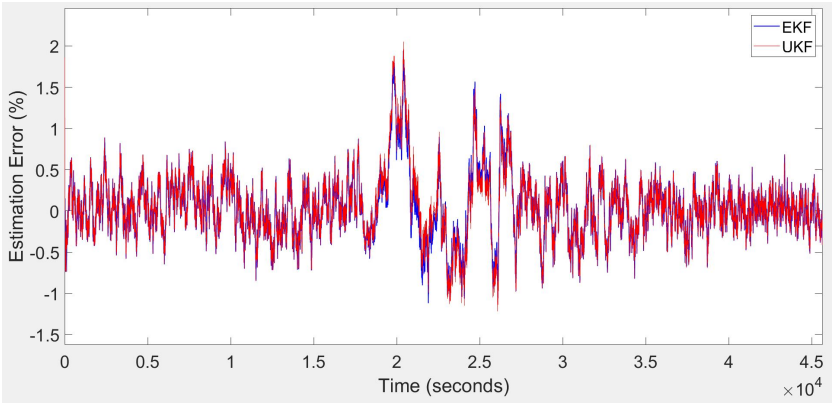

Figure 5.2: HPPC test - Estimation error for Linear model at 298.15 K.

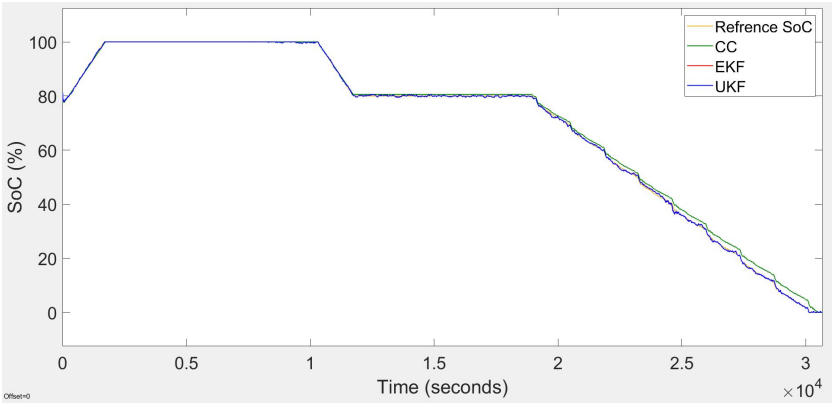

Figure 5.3: FUDS test - SoC estimation for Linear model at 298.15 K.

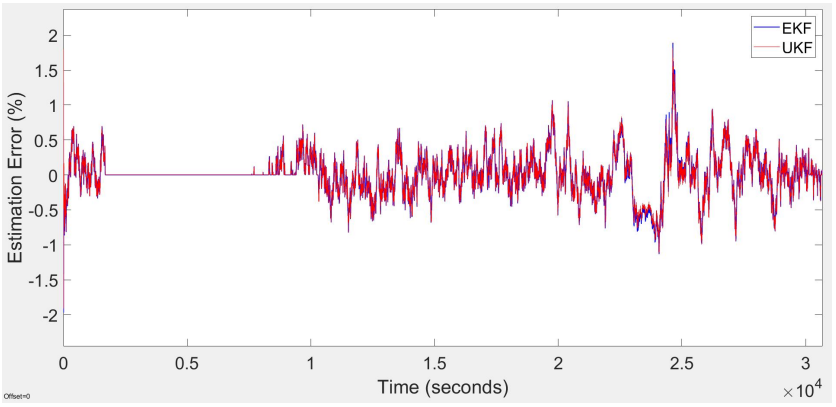

Figure 5.4: FUDS test - Estimation error for Linear model at 298.15 K.

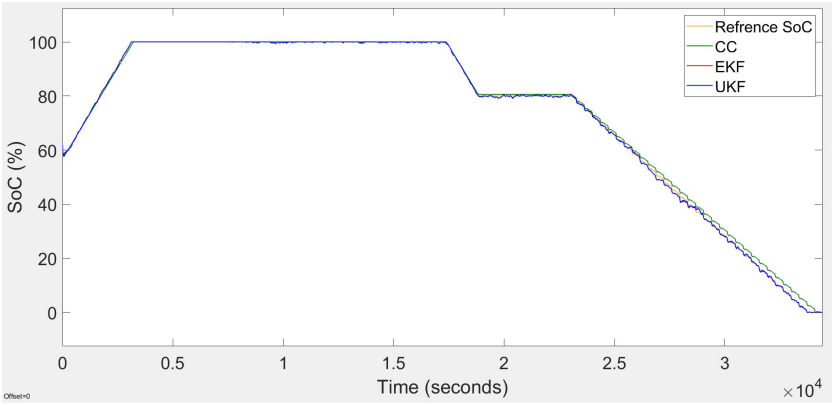

Figure 5.5: DST test - SoC estimation for Linear model at 298.15 K.

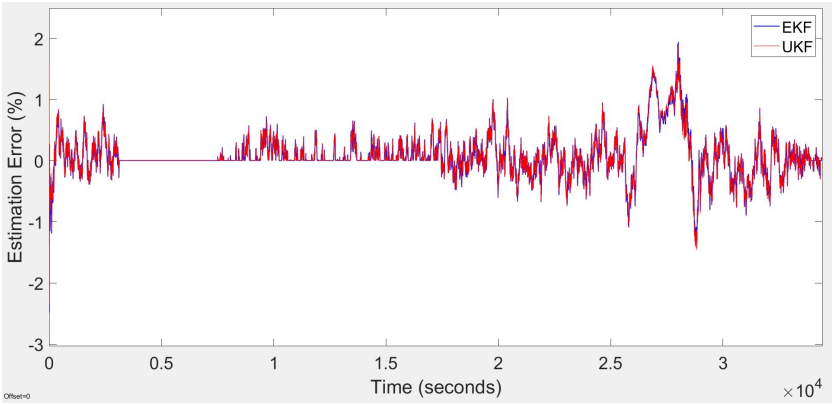

Figure 5.6: DST test - Estimation error for Linear model at 298.15 K.

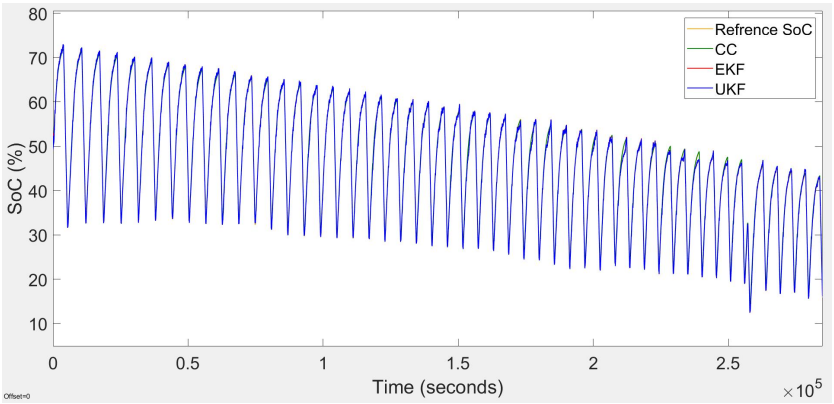

Figure 5.7: Constant current cycling test - SoC estimation for Linear model at 298.15 K.

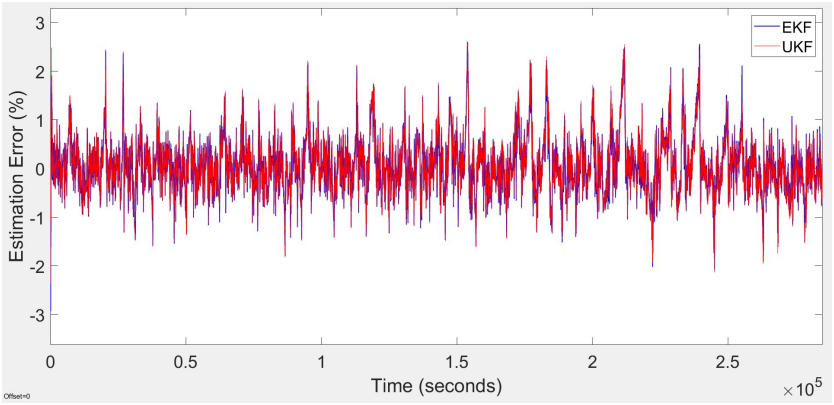

Figure 5.8: Constant current cycling test - Estimation error for Linear model at 298.15 K.

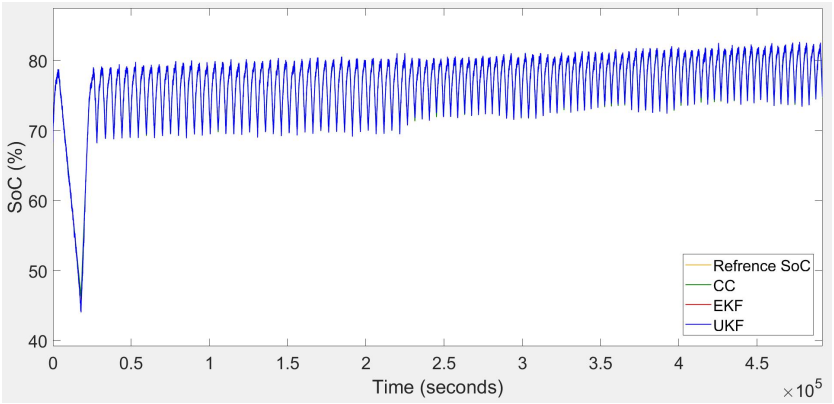

Figure 5.9: High regime cycling test - SoC estimation for Linear model at 298.15 K.

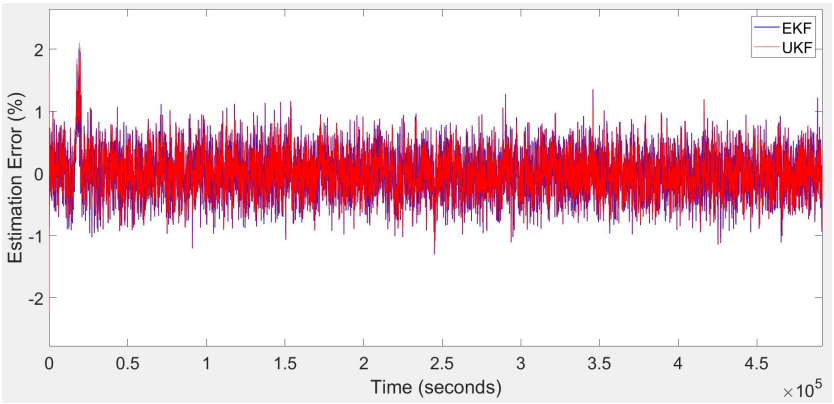

Figure 5.10: High regime cycling test - Estimation error for Linear model at 298.15 K.

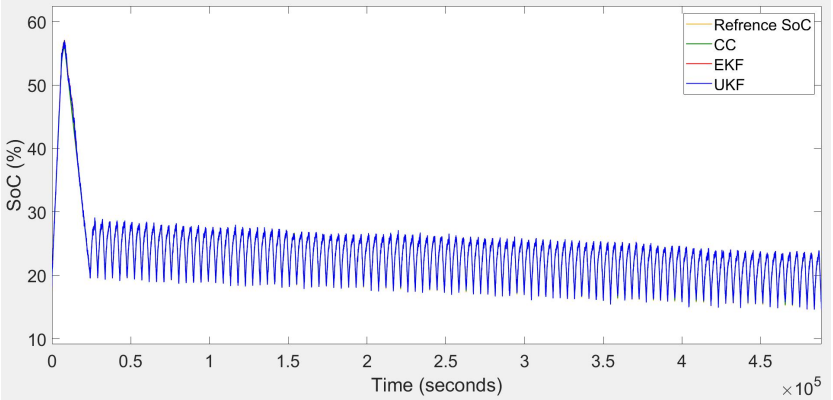

Figure 5.11: Low regime cycling test - SoC estimation for Linear model at 298.15 K.

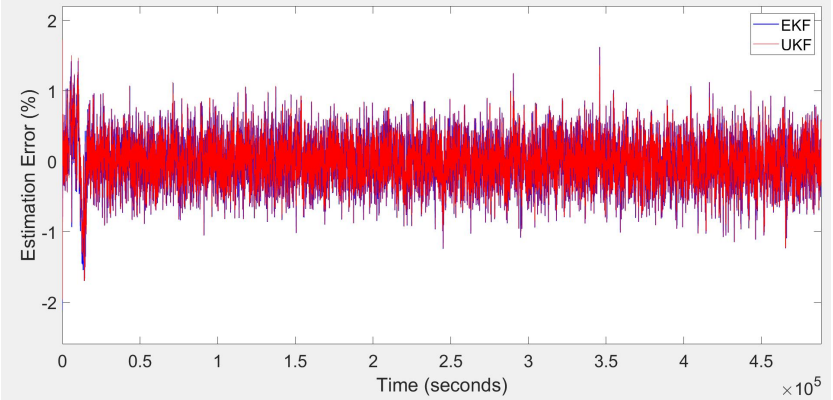

Figure 5.12: Low regime cycling test - Estimation error for Linear model at 298.15 K.

Referring to the SoC estimation error results represented, it can be seen that estimation error increases in SoC range corresponding to 60 - 30% at all the test conditions. This means the data used to develop the Linear model suffers from inaccuracy in the mentioned range. The increase in the estimation error is compensated rapidly and the estimated SoC value converge to the reference value.

Additionally, it is seen that in all the test conditions the estimation error is relatively higher in the initialization stage. This is because of the inaccuracy in the initial estimated system state which can be enhanced by optimizing the estimator tuning parameters and providing more accurate initialization predictions. The estimation error at the initialization stage reduces rapidly as the estimators execute the recursive state estimation approach.

In order to be able to compare the performance of the EKF and UKF estimators, the plot statistics of estimation error at 298.15 K (25°C) are given in Table 5.1, which includes the estimation error mean and standard deviation for the different test conditions.

Table 5.1: Plot Statistics of SoC Estimation Error for Linear Model at 298.15 K.

Battery Testing Profiles	Estimation Error Plot Statistics (%)			
	EKF		UKF	
	Mean	Standard Deviation	Mean	Standard Deviation
HPPC	0.046	0.37	0.049	0.38
FUDS	0.010	0.28	0.011	0.28
DST	0.077	0.33	0.077	0.34
Constant Current Cycling (1C)	0.070	0.53	0.072	0.53
High Regime Cycling	0.006	0.31	0.008	0.31
Low Regime Cycling	-0.004	0.29	-0.006	0.29

According to the data reported in Table 5.1, it can be concluded that for EKF estimator performs with higher accuracy due to lower error mean value. Consequently, the EKF estimator can be the optimal solution when the Linear model is employed for the Model-based SoC estimation.

For further assessment of the EKF and UKF estimator performance, the maximum estimation error for the Linear model at different test conditions and temperatures are summarized in Table 5.2.

In some test conditions, the maximum estimation error reported for the UKF estimator is lower in comparison to the EKF. However, by referring to the results obtained from comparing the estimation error mean value in Table 5.1, it can be concluded that, although the maximum error for UKF is lower, the error rate is consistently higher with respect to the EKF.

Table 5.2: Maximum SoC Estimation Error for Linear Model at Different Test Conditions and Temperatures.

Battery Testing Profiles	The SoC Estimation Error (%)							
	288.15 K		298.15 K		308.15 K		318.15 K	
	EKF	UKF	EKF	UKF	EKF	UKF	EKF	UKF
HPPC	1.84	1.84	1.94	2.05	1.90	2.00	1.97	2.01
FUDS	1.97	1.93	1.97	1.91	2.16	2.05	2.06	2.02
DST	2.67	2.50	2.48	2.35	2.39	2.27	2.37	2.23
Constant Current Cycling (1C)	3.05	3.03	2.93	2.59	2.96	2.80	2.70	2.68
High Regime Cycling	2.25	2.25	2.20	2.23	2.21	2.43	2.07	2.07
Low Regime Cycling	2.14	2.06	2.11	1.95	2.13	1.92	2.18	2.19

By analyzing the results, it has been observed that the maximum estimation error is related to the Constant Current Cycling test at 288.15 K which is bounded to 3%. The minimum estimation error is equal to 1.84% achieved with HPPC test at 288.15 K.

The error rate of 3% for SoC estimation is acceptable for most of the real-life BESS solutions. Consequently, For the NMC battery cell technology, the Model-based SoC estimation with Linear Model and the EKF estimator can produce SoC estimations with adequate accuracy.

5.2 Results for First-order Thevenin Model

The test results related to the first-order Thevenin model are represented at 298.15 K (25° C) in Figure 5.13 - Figure 5.24 that include both the SoC estimation and corresponding estimation error compared to the reference SoC.

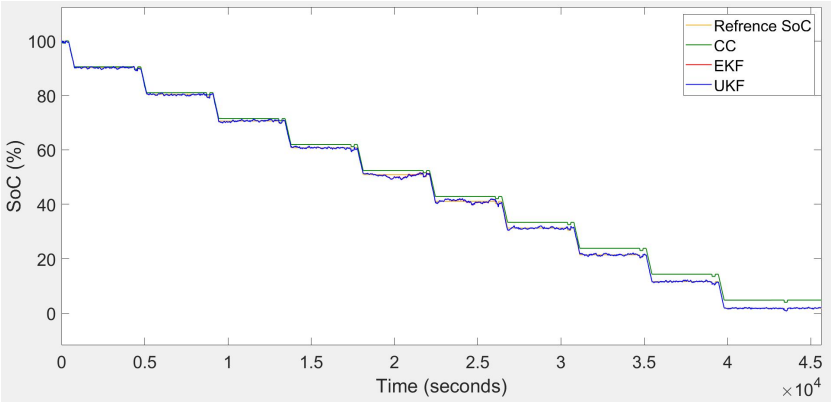

Figure 5.13: HPPC test - SoC estimation for first-order Thevenin model at 298.15 K.

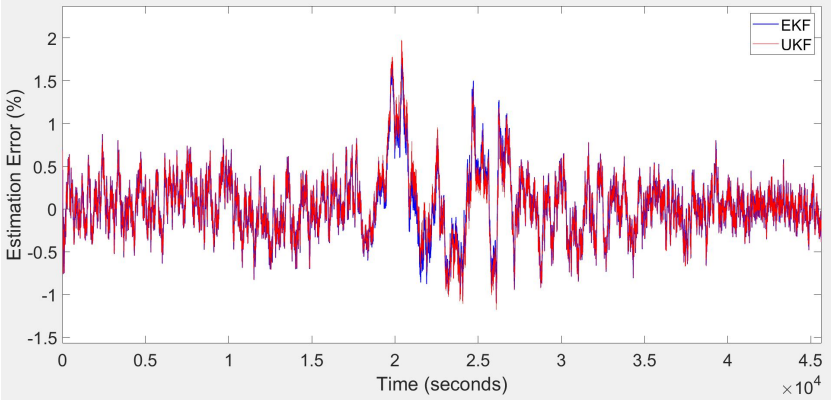

Figure 5.14: HPPC test - Estimation error for first-order Thevenin model at 298.15 K.

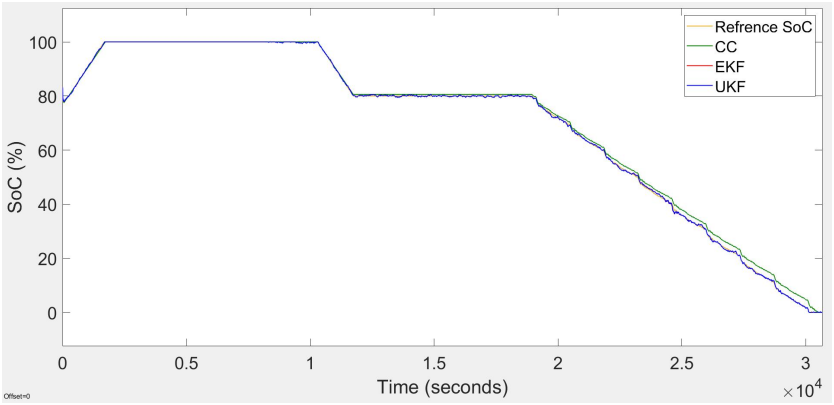

Figure 5.15: FUDS test - SoC estimation for first-order Thevenin model at 298.15 K.

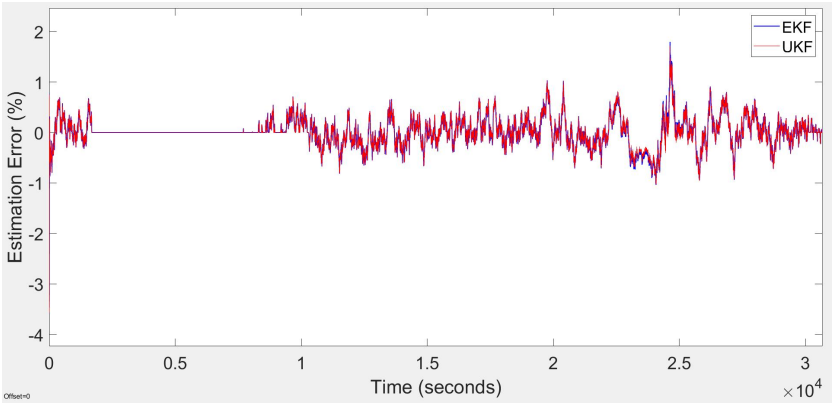

Figure 5.16: FUDS test - Estimation error for first-order Thevenin model at 298.15 K.

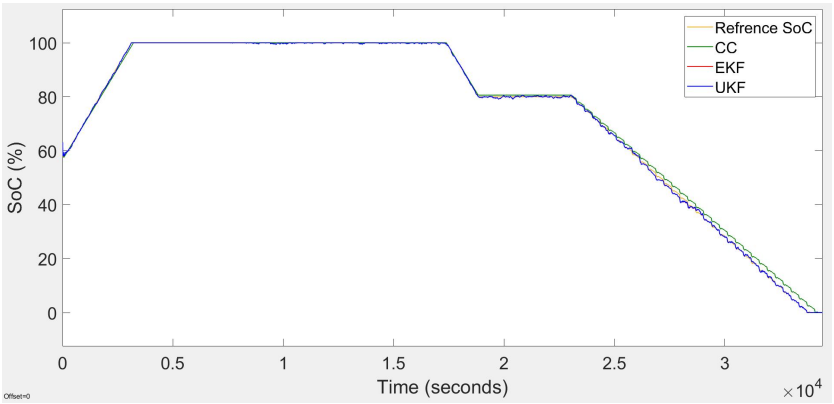

Figure 5.17: DST test - SoC estimation for first-order Thevenin model at 298.15 K.

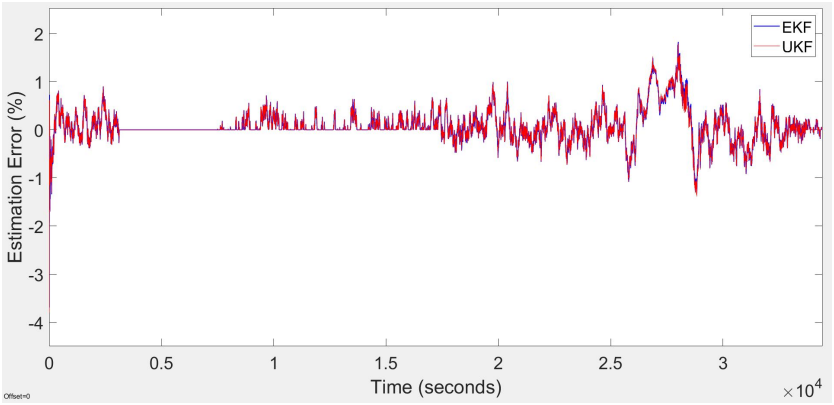

Figure 5.18: DST test - Estimation error for first-order Thevenin model at 298.15 K.

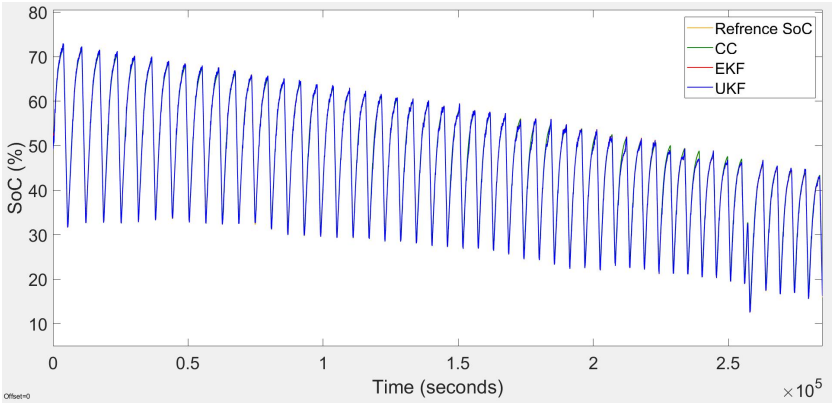

Figure 5.19: Constant current cycling test - SoC estimation for first-order Thevenin model at 298.15 K.

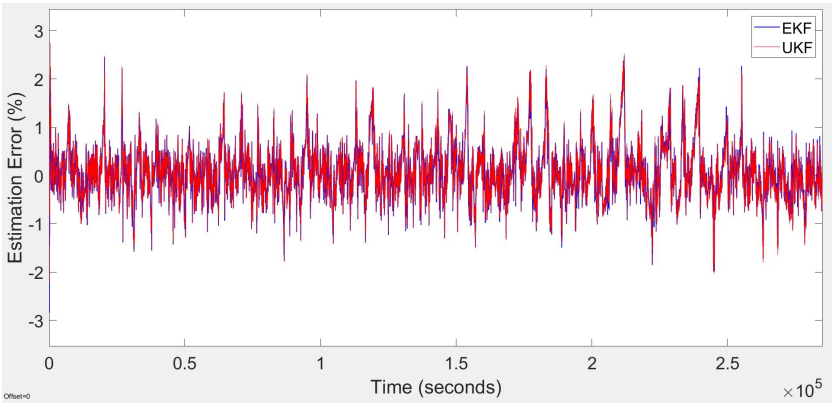

Figure 5.20: Constant current cycling test - Estimation error for first-order Thevenin model at 298.15 K.

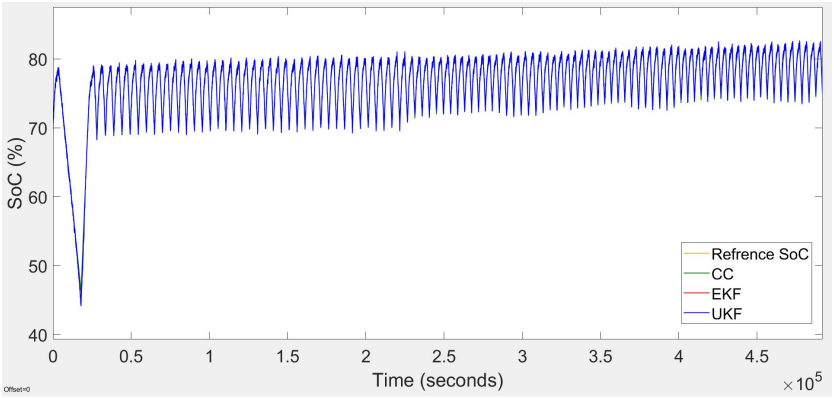

Figure 5.21: High regime cycling test - SoC estimation for first-order Thevenin model at 298.15 K.

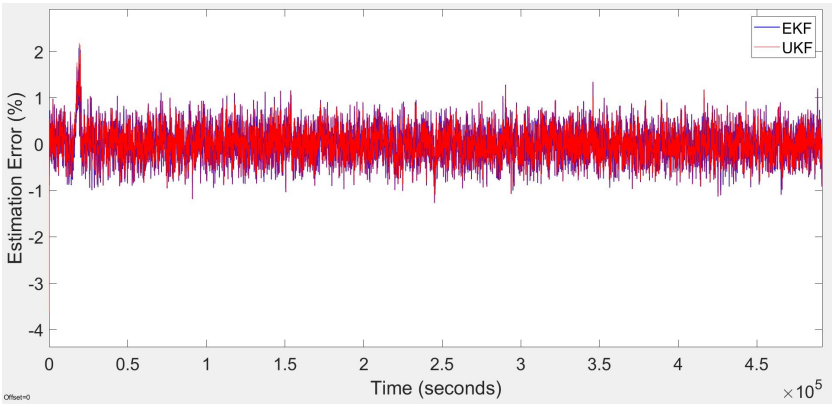

Figure 5.22: High regime cycling test - Estimation error for first-order Thevenin model at 298.15 K.

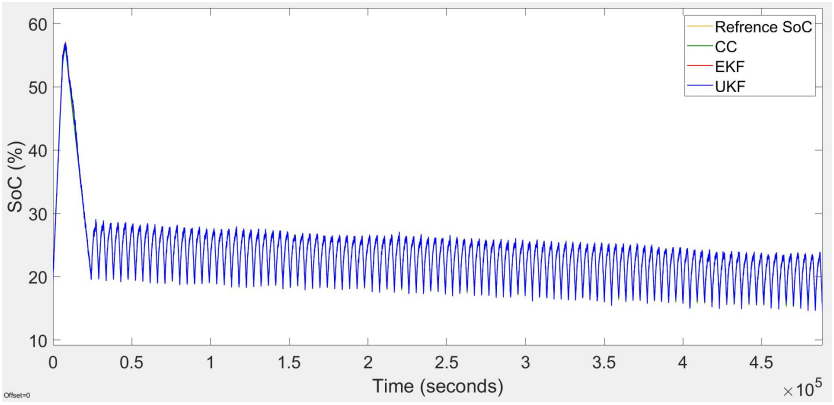

Figure 5.23: Low regime cycling test - SoC estimation for first-order Thevenin model at 298.15 K.

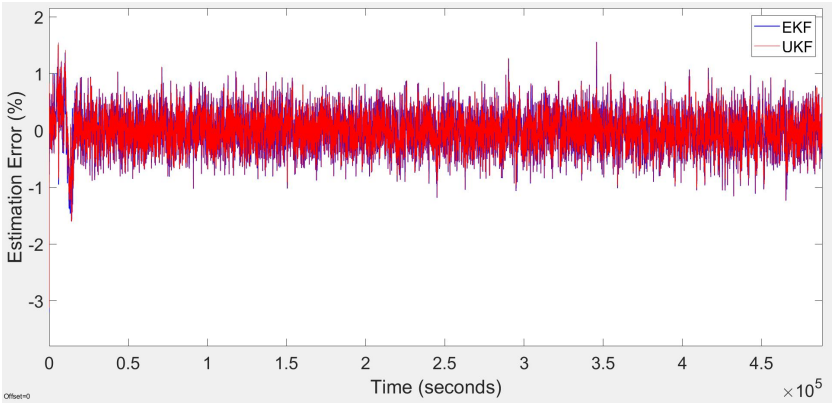

Figure 5.24: Low regime cycling test - Estimation error for first-order Thevenin model at 298.15 K.

By observing the SoC estimation results, it can be seen that the high estimation error rate in the initialization stage and SoC range 60 - 30% are repeating similar to the results obtained for the Linear Model in the previous section. This confirms that the inaccuracy in battery cell modeling has a considerable impact on the precision of the SoC estimation.

To compare the performance of the EKF and UKF estimators employed for the first-order Thevenin model, the estimation error mean and standard deviation for each test condition at 298.15 K is reported in Table 5.3.

Table 5.3: Plot Statistics of SoC Estimation Error for First-Order Thevenin Model at 298.15 K.

Battery Testing Profiles	Estimation Error Plot Statistics (%)			
	EKF		UKF	
	Mean	Standard Deviation	Mean	Standard Deviation
HPPC	0.044	0.36	0.048	0.36
FUDS	0.010	0.27	0.011	0.27
DST	0.072	0.32	0.072	0.33
Constant Current Cycling (1C)	0.076	0.52	0.078	0.52
High Regime Cycling	0.006	0.30	0.009	0.30
Low Regime Cycling	-0.004	0.29	-0.006	0.29

The results show that the SoC estimations produced by EKF have lower error rate in comparison to the UKF estimations. Therefore, it can be concluded that the EKF estimator can perform better when the first-order Thevenin model is hired for the Model-based SoC estimation.

To evaluate the EKF and UKF performance at different temperatures, the maximum estimation error for the first-order Thevenin model at different test conditions

are summarized in Table 5.4.

Table 5.4: Maximum SoC Estimation Error for First-order Thevenin Model at Different Test Conditions and Temperatures.

Battery Testing Profiles	The SoC Estimation Error (%)							
	288.15 K		298.15 K		308.15 K		318.15 K	
	EKF	UKF	EKF	UKF	EKF	UKF	EKF	UKF
HPPC	1.69	1.73	1.87	1.98	1.81	1.94	1.81	1.91
FUDS	3.49	3.59	3.47	3.56	3.48	3.57	3.05	3.60
DST	3.40	3.49	3.69	3.79	3.74	3.84	3.72	3.80
Constant Current Cycling (1C)	2.91	2.89	2.84	2.79	2.78	2.95	2.65	2.58
High Regime Cycling	3.61	3.59	3.65	3.65	3.63	3.64	3.57	3.58
Low Regime Cycling	3.34	3.35	3.20	3.12	3.19	2.97	3.10	2.77

The maximum estimation error (3.84%) occurs with the DST test condition at 308.15 K, and the minimum estimation error equal to 1.69% is recorded for the HPPC test at 288.15 K.

5.3 Results for Second-order Thevenin Model

The test results for the second-order Thevenin model are illustrated at 298.15 K (25° C) in Figure 5.25 - Figure 5.36 that include both the SoC estimation and corresponding estimation error compared to the reference SoC.

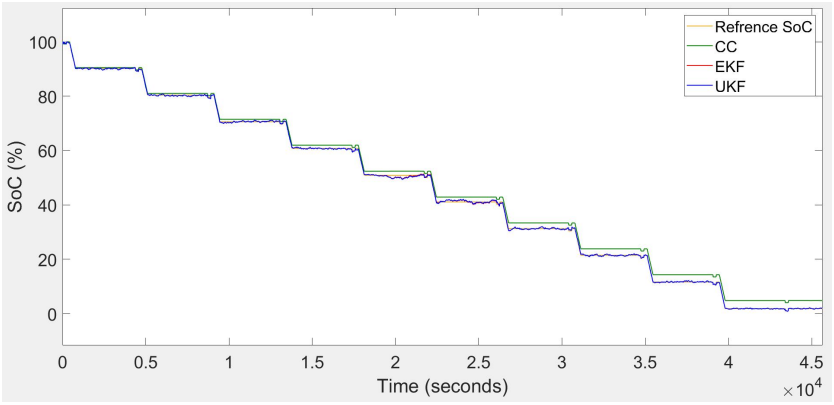

Figure 5.25: HPPC test - SoC estimation for second-order Thevenin model at 298.15 K.

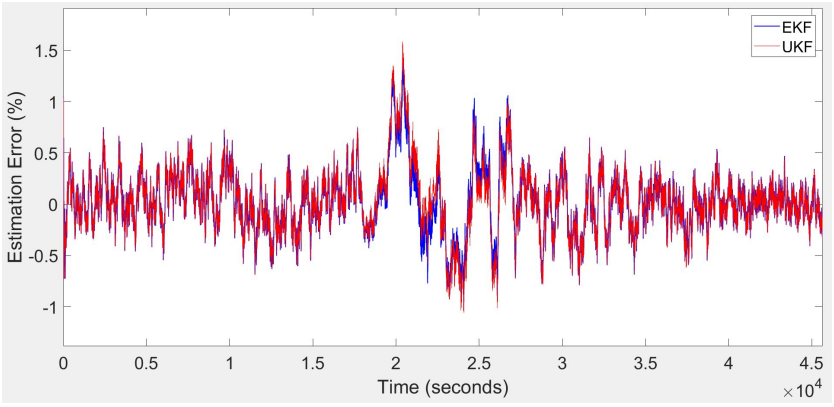

Figure 5.26: HPPC test - Estimation error for second-order Thevenin model at 298.15 K.

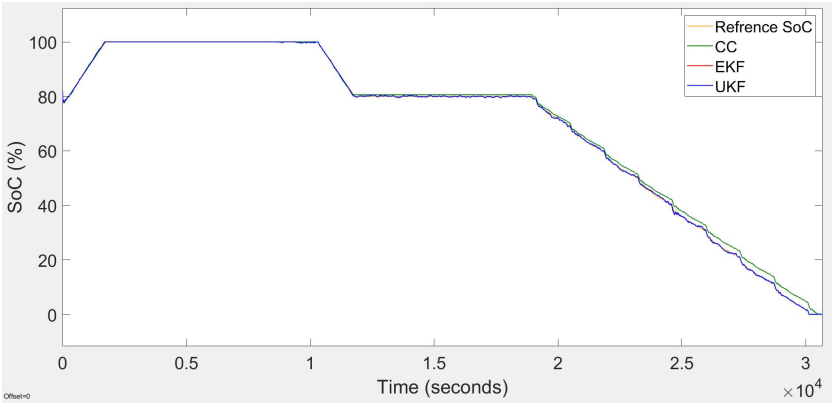

Figure 5.27: FUDS test - SoC estimation for second-order Thevenin model at 298.15 K.

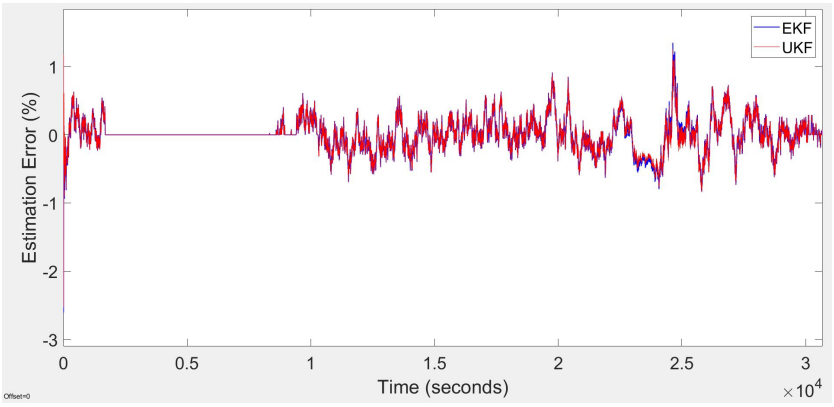

Figure 5.28: FUDS test - Estimation error for second-order Thevenin model at 298.15 K.

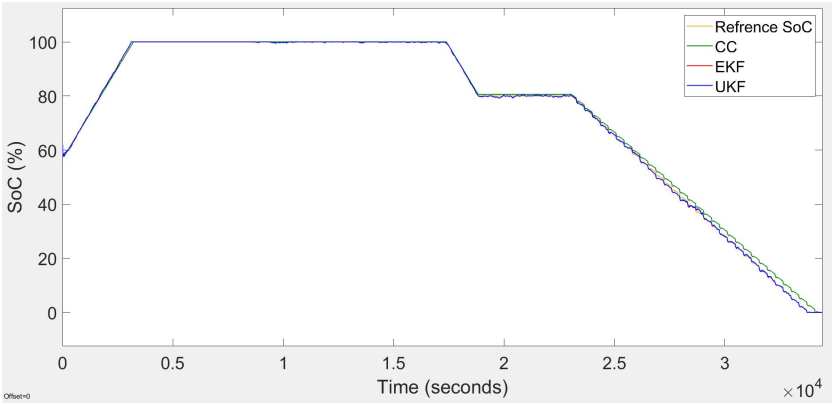

Figure 5.29: DST test - SoC estimation for second-order Thevenin model at 298.15 K.

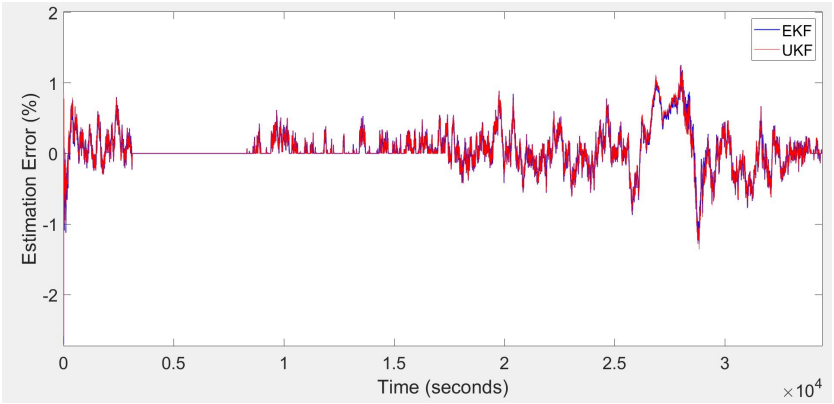

Figure 5.30: DST test - Estimation error for second-order Thevenin model at 298.15 K.

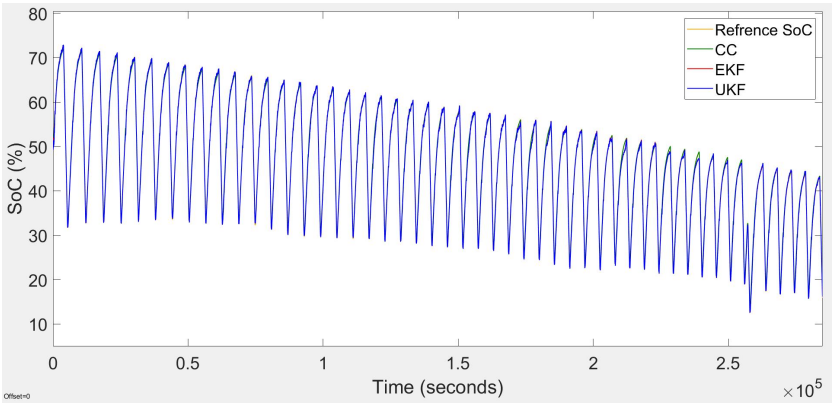

Figure 5.31: Constant current cycling test - SoC estimation for second-order Thevenin model at 298.15 K.

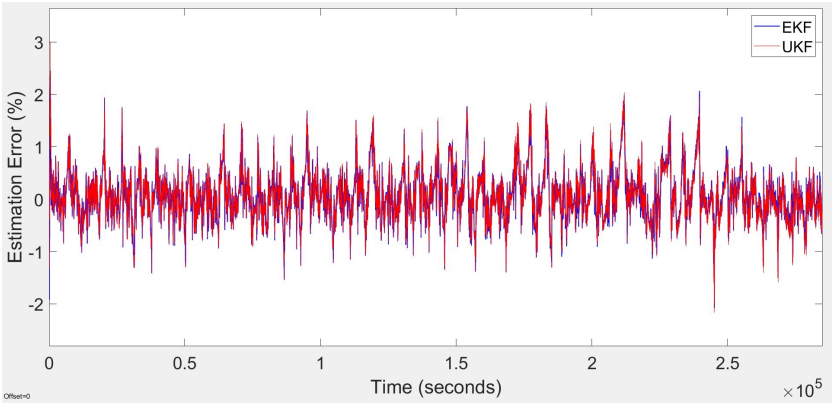

Figure 5.32: Constant current cycling test - Estimation error for second-order Thevenin model at 298.15 K.

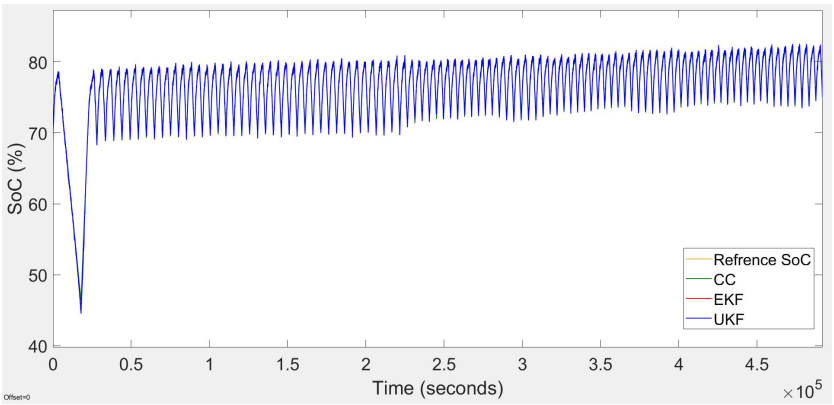

Figure 5.33: High regime cycling test - SoC estimation for second-order Thevenin model at 298.15 K.

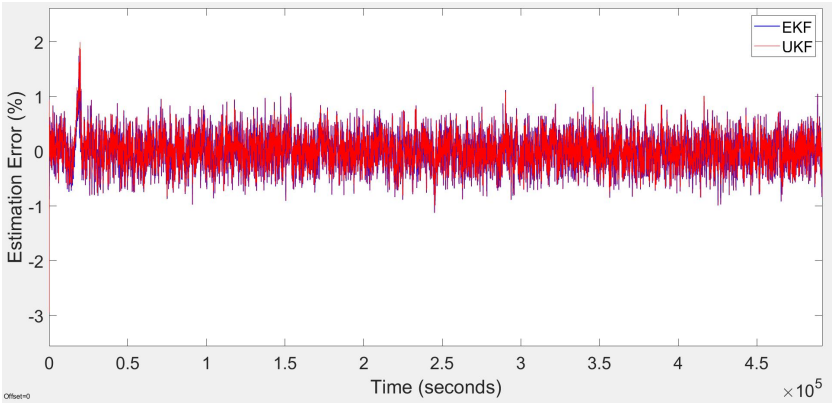

Figure 5.34: High regime cycling test - Estimation error for second-order Thevenin model at 298.15 K.

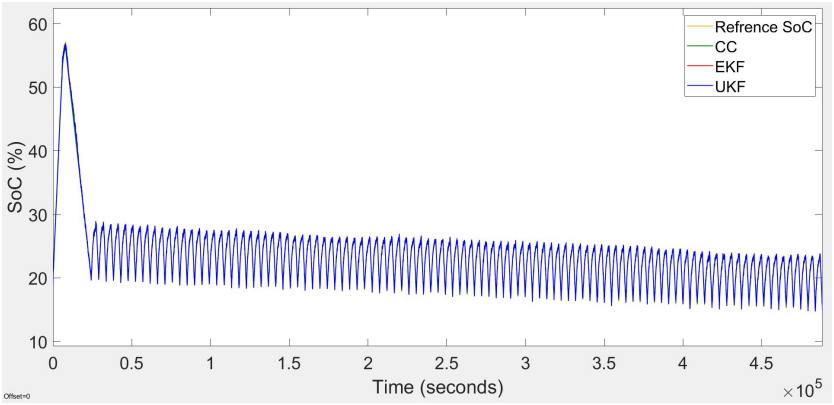

Figure 5.35: Low regime cycling test - SoC estimation for second-order Thevenin model at 298.15 K.

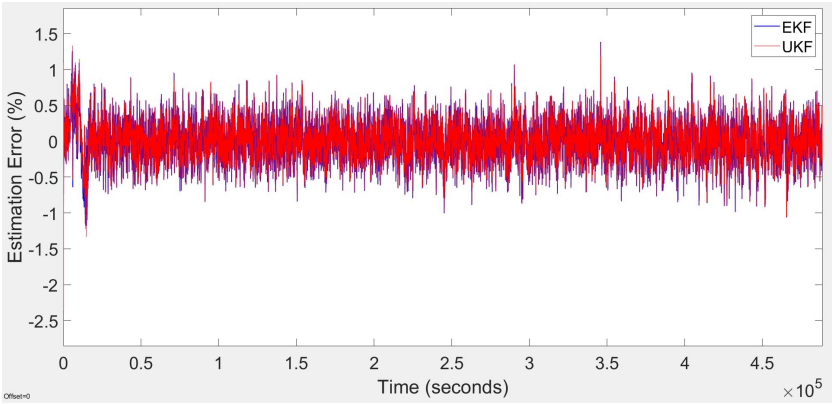

Figure 5.36: Low regime cycling test - Estimation error for second-order Thevenin model at 298.15 K.

The estimation error plot statistics, including the mean and standard deviation, for the second-order Thevenin model at 298.15, are reported in Table 5.5.

By comparing the performance of the EKF and UKF algorithms, it has been observed that EKF estimations have a lower error rate, suggesting that the linearization technique implemented by the EKF estimator is more efficient when is it is used in integration with the second-order Thevenin model.

Table 5.5: Plot Statistics of SoC Estimation Error for Second-Order Thevenin Model at 298.15 K.

Battery Testing Profiles	Estimation Error Plot Statistics (%)			
	EKF		UKF	
	Mean	Standard Deviation	Mean	Standard Deviation
HPPC	0.026	0.29	0.029	0.31
FUDS	0.005	0.23	0.006	0.22
DST	0.052	0.26	0.053	0.27
Constant Current Cycling (1C)	0.070	0.43	0.073	0.44
High Regime Cycling	0.005	0.26	0.008	0.27
Low Regime Cycling	0.002	0.24	0.006	0.24

EKF and UKF performance is also evaluated at different temperatures. The maximum estimation error for the second-order Thevenin model at different test conditions and temperatures are summarized in Table 5.6.

Table 5.6: Maximum SoC Estimation Error for Second-order Thevenin Model at Different Test Conditions and Temperatures.

Battery Testing Profiles	The SoC Estimation Error (%)							
	288.15 K		298.15 K		308.15 K		318.15 k	
	EKF	UKF	EKF	UKF	EKF	UKF	EKF	UKF
HPPC	1.36	1.41	1.46	1.58	1.46	1.59	1.31	1.41
FUDS	2.75	2.65	2.60	2.53	2.62	2.55	2.61	2.56
DST	2.67	2.45	2.70	2.58	2.62	2.54	2.36	2.28
Constant Current Cycling (1C)	2.19	2.28	2.35	3.00	2.48	3.23	2.55	2.99
High Regime Cycling	3.01	2.98	2.94	2.94	2.92	2.93	2.77	2.79
Low Regime Cycling	2.72	2.72	2.39	2.36	2.25	2.10	2.13	2.24

The results suggest that the maximum estimation error is related to the Constant current cycling test at 308.15 K with 3.23%, and the minimum error achieved is equal to 1.31% for the HPPC test at 318.15 K. According to the maximum error rate and the error mean values reported in Table 5.5 and Table 5.6, it can be concluded that the second-order Thevenin model has the highest accuracy with respect to the two other models analyzed earlier.

Further discussions regarding the results obtained for different models at different test conditions and the temperature is given in the next section.

5.4 Summary of the Results

Referring to the results represented earlier, it can be inferred that the performance of the Model-based SoC estimation structures developed for this study is affected by different factors, such as C-rate, temperature, and the estimator tuning parameters.

Considering the HPPC test results reported in Table 5.2, Table 5.4 and Table 5.6, it is be observed that the accuracy of the SoC estimation for all the models, is higher compared to the other test conditions. Accordingly, for the HPPC test condition at different temperatures, the estimation error is bounded to 2%. This is due to the fact that the battery cell models are developed based on the HPPC test profile and data. Therefore, the battery cell model performance and accuracy are much higher with respect to the other test conditions.

The estimation errors more than 3% do not disqualify the model based SoC estimations developed for the present study and the error rate can be possibly decreased by providing more accurate initialization data and assigning optimum tuning parameters. Accordingly, both the EKF and UKF estimators are capable to successfully produce SoC estimations with an error below of 3%, which is required by most modern industrial applications.

By comparing the results published in previous sections, it can be inferred that the SoC estimations regarding the second-order Thevenin model show higher accuracy. This wasn't out of expectation as it has been discussed that the second-order Thevenin model is able to simulate the nonlinear characteristics of the battery cell with high fidelity. However, this result doesn't disqualify the Linear model and the first-order Thevenin model since the results achieved for these models have the acceptable accuracy.

It is worth noting that, at some test conditions, the results regarding the linear model indicate higher accuracy with respect to the results for first-order Thevenin model. This can be explained considering that adding one RC pairs to the battery model increases the uncertainties as well as the model fidelity. The uncertainties corresponding to the added RC pair are parameterized within the process and measurement noise covariance matrices. In other words, it is possible to achieve better results using the first-order Thevenin model, if the tuning parameters are set optimally, which was not possible to be done at this stage, as the present study is aiming to compare the model-based SoC estimation algorithms with identical tuning parameters.

By analyzing the results achieved from repeating the tests at different temperatures it can be seen that the temperature variation influences the SoC estimation. It's safe to say that the temperature doesn't affect the SoC estimators performance. However, the temperature has a direct effect on the battery cell itself which is also reflected by the battery cell models. Meaning that, the battery cell models are responsible for the changes in SoC estimation accuracy with respect to the temperature.

As it was mentioned before, the results regarding the CC algorithm suffers from

integration error through the time. This can be clearly observed by referring to the HPPC, FUDS, and DST SoC estimation results. However, the maximum estimation error for the CC is lower for the Constant Current cycling, High regime cycling and Low regime cycling tests since the frequent charging and discharging process prevents from integrating the error over long period of time. The long-term drift in SoC estimated by CC cannot be corrected due to the lack of a reference point and the error rate increases as the CE is set to lower values.

CE has direct effect on the EKF and UKF estimations as well. It is evident that benefiting from higher efficiency would lead to better estimation results. For NMC batteries the CE is typically ranged between 95 - 99% depending on the electrolyte chemistry and the battery age.

The results approve that, for the NMC battery chemistry, which has mild nonlinear characteristics, the EKF estimator can be the optimal solution due to its higher precision and lower computational load. The latter reveals that the UKF estimator is not necessarily the most accurate estimator for every battery cell type.

Chapter 6

Conclusions and Future Works

This thesis represents the inclusive study of different Model-based SoC estimation structures aiming to identify the best trade-off between the model and estimator complexity and accuracy as well as providing more clear insight into the advantages and disadvantages of each structure.

To achieve the study objectives, the Model-based structures were developed for the NMC battery cell by using Linear model, first-order Thevenin model and the second-order Thevenin model in integration with EKF and UKF estimators, which are the most frequently implemented SoC estimation algorithms in the literature.

The performance of the battery cell models are validated at different temperatures. The indications represented that the models developed based on the data collected from the HPPC tests at 318.15 K (45° C) benefit from higher accuracy as the higher temperature enhances battery cell performance from electrochemical point of view.

Different test profiles and conditions, which tend to simulate the real-life application requirements, were used to provide meaningful comparison and evaluation of each SoC estimation structure.

By referring to the results obtained at different conditions, it has been observed that the Model-based SoC estimation with second-order Thevenin model and the EKF estimator performed with higher accuracy. This can be explained by pointing out that the model accuracy plays a key role in Model-based SoC estimation and the second-order Thevenin model is able to simulate the real battery cell with higher physical correspondence and fidelity. Moreover, the EKF estimator that benefits from linearization technique based on the first-order Taylor series expansion performs better for the NMC battery chemistry, which is characterized by mild non-linearity.

The results achieved with the other battery cell models revealed that both EKF and UKF can successfully estimate the SoC with adequate accuracy. Therefore, it can be concluded that different Model-based SoC structures can be implemented with respect to real-life application requirements and constraints. In other words, for applications with limited computational resources or lower accuracy requirements,

the Linear or first-order Thevenin model can be employed ensuring that the SoC estimation will not be affected drastically.

During the simulation procedure, it has been observed that the EKF and UKF performance can be optimized by adjusting the tuning parameters. Therefore, it is possible to minimize the estimation error if the EKF and UKF estimators are tuned independently considering each battery cell model.

Further research on developing a novel technique to extract the optimal tuning parameters for EKF and UKF estimators is suggested future work.

The battery cell models can be improved by modeling the effective capacity at different C-rates and temperatures, the effect of the battery self-discharging and the effect of Hysteresis phenomena. Furthermore, conducting more tests for sensitivity analysis and studying the effect of each tuning parameter on the SoC estimation is advised.

Finally, it is also recommended to develop a hybrid SoC estimation method combining the Model-based structure and AI algorithms to enhance the online SoC estimation by reducing the EKF and UKF run time and frequency.

Bibliography

[1] C. Parthasarathy, H. Hafezi, and H. Laaksonen. Lithium-ion bess integration for smart grid applications - ecm modelling approach. In *2020 IEEE Power Energy Society Innovative Smart Grid Technologies Conference (ISGT)*, pages 1–5, 2020.

[2] Gregory L Plett. *Battery management systems. Volume II, Equivalent-circuit methods*. Artech House, 2016.

[3] Akira Yoshino. 1 - development of the lithium-ion battery and recent technological trends. In Gianfranco Pistoia, editor, *Lithium-Ion Batteries*, pages 1 – 20. Elsevier, Amsterdam, 2014.

[4] Hideaki Horie. 5 - evs and hevs: The need and potential functions of batteries for future systems. In Gianfranco Pistoia, editor, *Lithium-Ion Batteries*, pages 83 – 95. Elsevier, Amsterdam, 2014.

[5] Kevin G. Gallagher and Paul A. Nelson. 6 - manufacturing costs of batteries for electric vehicles. In Gianfranco Pistoia, editor, *Lithium-Ion Batteries*, pages 97 – 126. Elsevier, Amsterdam, 2014.

[6] N. J. Cammardella, R. W. Moye, Y. Chen, and S. P. Meyn. An energy storage cost comparison: Li-ion batteries vs distributed load control. In *2018 Clemson University Power Systems Conference (PSC)*, pages 1–6, 2018.

[7] W. Chen, Y. Liu, F. Shi, Q. An, C. Dai, and X. Fu. Review: Efficiency factors and optimization of lithium-ion battery. In *2019 14th IEEE Conference on Industrial Electronics and Applications (ICIEA)*, pages 644–649, 2019.

[8] Holger Hesse, Michael Schimpe, Daniel Kucevic, and Andreas Jossen. Lithium-ion battery storage for the grid—a review of stationary battery storage system design tailored for applications in modern power grids. *Energies*, 10(12):2107, Dec 2017.

[9] Cong Truong, Maik Naumann, Ralph Karl, Marcus Müller, Andreas Jossen, and Holger Hesse. Economics of residential photovoltaic battery systems in germany: The case of tesla's powerwall. *Batteries*, 2(2):14, May 2016.

[10] Hartmut Hinz. Comparison of lithium-ion battery models for simulating storage systems in distributed power generation. *Inventions*, 4(3):41, Aug 2019.

[11] Jagdesh Kumar, Chethan Parthasarathy, Mikko Västi, Hannu Laaksonen, Miadreza Shafie-Khah, and Kimmo Kauhaniemi. Sizing and allocation of battery energy storage systems in Åland islands for large-scale integration of renewables and electric ferry charging stations. *Energies*, 13(2):317, Jan 2020.

[12] Robert Salas-Puente, Silvia Marzal, Raul Gonzalez-Medina, Emilio Figueres, and Gabriel Garcera. Practical analysis and design of a battery management system for a grid-connected dc microgrid for the reduction of the tariff cost and battery life maximization. *Energies*, 11(7):1889, Jul 2018.

[13] L. Buccolini, A. Ricci, C. Scavongelli, G. DeMaso-Gentile, S. Orcioni, and M. Conti. Battery management system (bms) simulation environment for electric vehicles. In *2016 IEEE 16th International Conference on Environment and Electrical Engineering (EEEIC)*, pages 1–6, 2016.

[14] K. W. E. Cheng, B. P. Divakar, H. Wu, K. Ding, and H. F. Ho. Battery-management system (bms) and soc development for electrical vehicles. *IEEE Transactions on Vehicular Technology*, 60(1):76–88, 2011.

[15] J. Cabrera, A. Vega, F. Tobajas, V. Déniz, and H. A. Fabelo. Design of a reconfigurable li-ion battery management system (bms). In *2014 XI Tecnologias Aplicadas a la Ensenanza de la Electronica (Technologies Applied to Electronics Teaching) (TAEE)*, pages 1–6, 2014.

[16] Juan Rivera-Barrera, Nicolás Muñoz-Galeano, and Henry Sarmiento-Maldonado. Soc estimation for lithium-ion batteries: Review and future challenges. *Electronics*, 6(4):102, Nov 2017.

[17] Ruifeng Zhang, Bizhong Xia, Baohua Li, Yongzhi Lai, Weiwei Zheng, Huawen Wang, Wei Wang, and Mingwang Wang. Study on the characteristics of a high capacity nickel manganese cobalt oxide (nmc) lithium-ion battery—an experimental investigation. *Energies*, 11(9):2275, Aug 2018.

[18] D. N. T. How, M. A. Hannan, M. S. Hossain Lipu, and P. J. Ker. State of charge estimation for lithium-ion batteries using model-based and data-driven methods: A review. *IEEE Access*, 7:136116–136136, 2019.

[19] Y. Zhou and X. Li. Overview of lithium-ion battery soc estimation. In *2015 IEEE International Conference on Information and Automation*, pages 2454–2459, 2015.

[20] Alberto Berrueta, Andoni Urtasun, Alfredo Ursúa, and Pablo Sanchis. A comprehensive model for lithium-ion batteries: From the physical principles to an electrical model. *Energy*, 144:286 – 300, 2018.

[21] Jinhao Meng, Guangzhao Luo, Mattia Ricco, Maciej Swierczynski, Daniel-Ioan Stroe, and Remus Teodorescu. Overview of lithium-ion battery modeling methods for state-of-charge estimation in electrical vehicles. *Applied Sciences*, 8(5):659, Apr 2018.

[22] Wei He, Michael Pecht, David Flynn, and Fateme Dinmohammadi. A physics-based electrochemical model for lithium-ion battery state-of-charge estimation solved by an optimised projection-based method and moving-window filtering. *Energies*, 11(8):2120, Aug 2018.

[23] Peng Rong and Massoud Pedram. An analytical model for predicting the remaining battery capacity of lithium-ion batteries. volume 14, 03 2003.

[24] Gaizka Saldaña, José Ignacio San Martín, Inmaculada Zamora, Francisco Javier Asensio, and Oier Oñederra. Analysis of the current electric battery models for electric vehicle simulation. *Energies*, 12(14):2750, Jul 2019.

[25] Martin Murnane and Adel Ghazel. A closer look at state of charge (soc) and state of health (soh) estimation techniques for batteries. 2017.

[26] M. Garmendia, I. Gandiaga, G. Perez, U. Viscarret, and I. Etxeberria-Otadui. Proposal and validation of a soc estimation algorithm of lifepo4 battery packs for traction applications. *World Electric Vehicle Journal*, 6(3):771–781, Sep 2013.

[27] Y. Tripathy, A. McGordon, J. Marco, and M. Gama-Valdez. State-of-charge estimation algorithms and their implications on cells in parallel. In *2014 IEEE International Electric Vehicle Conference (IEVC)*, pages 1–6, 2014.

[28] Yong Luo, Yingzhe Kan, Yanli Yin, Li Liu, Huanyu Cui, and Fei Wu. Study on a high-accuracy real-time algorithm to estimate soc of multiple battery cells simultaneously, Aug 2017.

[29] F. Ciortea, C. Rusu, M. Nemes, and C. Gatea. Extended kalman filter for state-of-charge estimation in electric vehicles battery packs. In *2017 International Conference on Optimization of Electrical and Electronic Equipment (OPTIM) 2017 Intl Aegean Conference on Electrical Machines and Power Electronics (ACEMP)*, pages 611–616, 2017.

[30] Dong Xile, Zhang Caiping, and Jiang Jiuchun. Evaluation of soc estimation method based on ekf/aekf under noise interference. *Energy Procedia*, 152:520 – 525, 2018. Cleaner Energy for Cleaner Cities.

[31] W. Wang, X. Wang, C. Xiang, C. Wei, and Y. Zhao. Unscented kalman filter-based battery soc estimation and peak power prediction method for power distribution of hybrid electric vehicles. *IEEE Access*, 6:35957–35965, 2018.

[32] Fang Liu, Jie Ma, and Weixing Su. Unscented particle filter for soc estimation algorithm based on a dynamic parameter identification, Apr 2019.

[33] Zhongyue Zou, Jun Xu, Chris Mi, Binggang Cao, and Zheng Chen. Evaluation of model based state of charge estimation methods for lithium-ion batteries. *Energies*, 7(8):5065–5082, Aug 2014.

[34] Behrooz Nemounehkhah, Roberto Faranda, Kishore Akkala, Hossein Hafezi, Chethan Parthasarathy, and Hannu Laaksonen. Comparison and evaluation of state of charge estimation methods for a verified battery model. *I*, page 6, 2020.

[35] Hongwen He, Hongzhou Qin, Xiaokun Sun, and Yuanpeng Shui. Comparison study on the battery soc estimation with ekf and ukf algorithms. *Energies*, 6(10):5088–5100, Sep 2013.

[36] Liang Feng, Jie Ding, and Yiyang Han. Improved sliding mode based ekf for the soc estimation of lithium-ion batteries. *Ionics*, 26(6):2875–2882, Feb 2020.

[37] Jiayi Luo, Jiankun Peng, and Hongwen He. Lithium-ion battery soc estimation study based on cubature kalman filter. *Energy Procedia*, 158:3421 – 3426, 2019. Innovative Solutions for Energy Transitions.

[38] Jiankun Peng, Jiayi Luo, Hongwen He, and Bing Lu. An improved state of charge estimation method based on cubature kalman filter for lithium-ion batteries. *Applied Energy*, 253:113520, 2019.

[39] Y. Song, M. Park, M. Seo, and S. W. Kim. Improved soc estimation of lithium-ion batteries with novel soc-ocv curve estimation method using equivalent circuit model. In *2019 4th International Conference on Smart and Sustainable Technologies (SpliTech)*, pages 1–6, 2019.

[40] M. A. Hannan, M. S. Hossain Lipu, Aini Hussain, Pin Jern Ker, T. M. I. Mahlia, M. Mansor, Afida Ayob, Mohamad H. Saad, and Z. Y. Dong. Toward enhanced state of charge estimation of lithium-ion batteries using optimized machine learning techniques. *Scientific Reports*, 10(1):1–15, Mar 2020.

[41] Wei Xu, Jinli Xu, Baolei Liu, Jiajun Liu, and Xiaofeng Yan. A multi-timescale adaptive dual particle filter for state of charge estimation of lithium-ion batteries considering temperature effect. *Energy Science Engineering*, Apr 2020.

[42] R. Arunachala, C. Parthasarathy, A. Jossen, and J. Garche. Inhomogeneities in large format lithium ion cells: A study by battery modelling approach. *ECS Transactions*, 73(1):201–212, sep 2016.

[43] Caiping Zhang, Jiuchun Jiang, Linjing Zhang, Sijia Liu, Leyi Wang, and Poh Loh. A generalized soc-ocv model for lithium-ion batteries and the soc estimation for lnmco battery. *Energies*, 9(11):900, Nov 2016.

[44] Yongling He, Rong He, Bin Guo, Zhengjie Zhang, Shichun Yang, Xinhua Liu, Xichang Zhao, Yuwei Pan, Xiaoyu Yan, and Shen Li. Modeling of dynamic hysteresis characters for the lithium-ion battery. *Journal of The Electrochemical Society*, 167(9):090532, may 2020.

[45] Abbas Fotouhi, Daniel J. Auger, Karsten Propp, Stefano Longo, and Mark Wild. A review on electric vehicle battery modelling: From lithium-ion toward lithium–sulphur. *Renewable and Sustainable Energy Reviews*, 56:1008 – 1021, 2016.

[46] Simone Barcellona and Luigi Piegari. Lithium ion battery models and parameter identification techniques. *Energies*, 10(12), 2017.

[47] Jinhao Meng, Guangzhao Luo, Mattia Ricco, Maciej Swierczynski, Daniel-Ioan Stroe, and Remus Teodorescu. Overview of lithium-ion battery modeling methods for state-of-charge estimation in electrical vehicles. *Applied Sciences*, 8(5), 2018.

[48] Nalin A. Chaturvedi, Reinhardt Klein, Jake Christensen, Jasim Ahmed, and Aleksandar Kojic. Algorithms for advanced battery-management systems. *IEEE Control Systems*, 30:49–68, 2010.

[49] A. A. Hussein and I. Batarseh. An overview of generic battery models. In *2011 IEEE Power and Energy Society General Meeting*, pages 1–6, 2011.

[50] Ehsan Samadani, Siamak Farhad, William Scott, Mehrdad Mastali, Leonardo E. Gimenez, Michael Fowler, and Roydon A. Fraser. Empirical modeling of lithium-ion batteries based on electrochemical impedance spectroscopy tests. *Electrochimica Acta*, 160:169 – 177, 2015.

[51] M. Charkhgard and M. Farrokhi. State-of-charge estimation for lithium-ion batteries using neural networks and ekf. *IEEE Transactions on Industrial Electronics*, 57(12):4178–4187, 2010.

[52] Muhammad Ali, Muhammad Kamran, Pandiyan Kumar, Himanshu, Sarvar Nengroo, Muhammad Khan, Altaf Hussain, and Hee-Je Kim. An online data-driven model identification and adaptive state of charge estimation approach for lithium-ion-batteries using the lagrange multiplier method. *Energies*, 11(11):2940, Oct 2018.

[53] G. S. Misyris, D. I. Doukas, T. A. Papadopoulos, D. P. Labridis, and V. G. Agelidis. State-of-charge estimation for li-ion batteries: A more accurate hybrid approach. *IEEE Transactions on Energy Conversion*, 34(1):109–119, 2019.

[54] Ines Baccouche, Sabeur Jemmali, Bilal Manai, Noshin Omar, and Najoua Amara. Improved ocv model of a li-ion nmc battery for online soc estimation using the extended kalman filter. *Energies*, 10(6):764, May 2017.

[55] Zhihao Yu, Ruituo Huai, and Linjing Xiao. State-of-charge estimation for lithium-ion batteries using a kalman filter based on local linearization. *Energies*, 8(8):7854–7873, Jul 2015.

[56] J. Xu, B. Cao, J. Cao, Z. Zou, C. C. Mi, and Z. Chen. A comparison study of the model based soc estimation methods for lithium-ion batteries. In *2013 IEEE Vehicle Power and Propulsion Conference (VPPC)*, pages 1–5, 2013.

[57] Dan Simon. *Optimal state estimation: Kalman, H [infinity symbol] and nonlinear approaches*. Wiley-Interscience, 2006.

[58] X. Wu, X. Li, and J. Du. State of charge estimation of lithium-ion batteries over wide temperature range using unscented kalman filter. *IEEE Access*, 6:41993–42003, 2018.

[59] P. Shi and Y. Zhao. Application of unscented kalman filter in the soc estimation of li-ion battery for autonomous mobile robot. In *2006 IEEE International Conference on Information Acquisition*, pages 1279–1283, 2006.

[60] Uscar: Usabc electric vehicle battery test procedures manual. `https://www.uscar.org/guest/article_view.php?articles_id=74`.

[61] Wei He, Nicholas Williard, Chaochao Chen, and Michael Pecht. State of charge estimation for li-ion batteries using neural network modeling and unscented kalman filter-based error cancellation. *International Journal of Electrical Power Energy Systems*, 62:783 – 791, 2014.

Appendix A

HPPC Test Results for Model Validation

The HPPC test results for battery cell model validation at temperature equal to 288.15 K and 318.15 K are represented below.

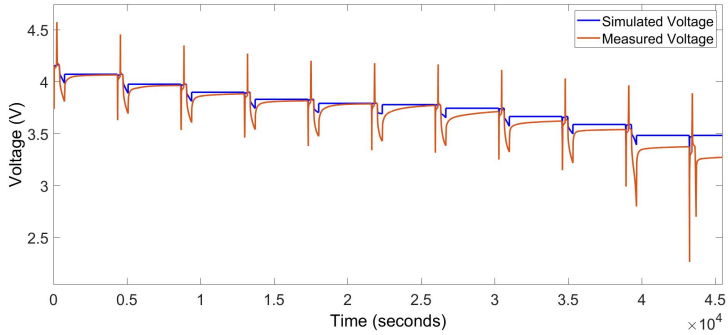

Figure A.1: HPPC test voltage for Linear model at 288.15 K.

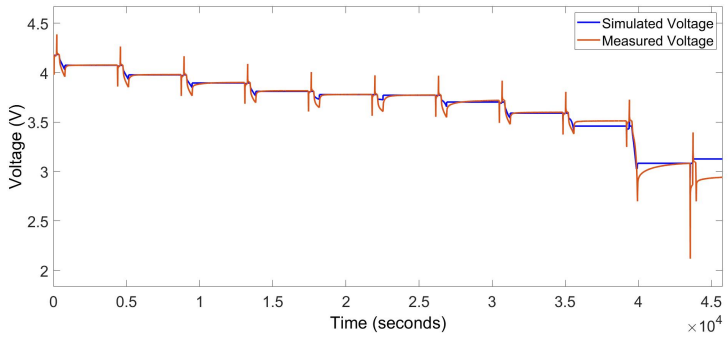

Figure A.2: HPPC test voltage for Linear model at 318.15 K.

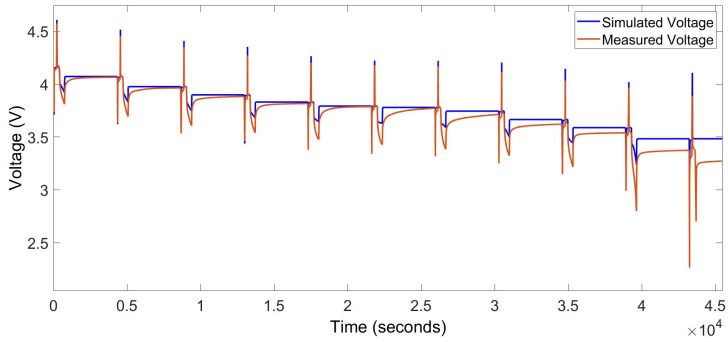

Figure A.3: HPPC test voltage for first-order Thevenin model at 288.15 K.

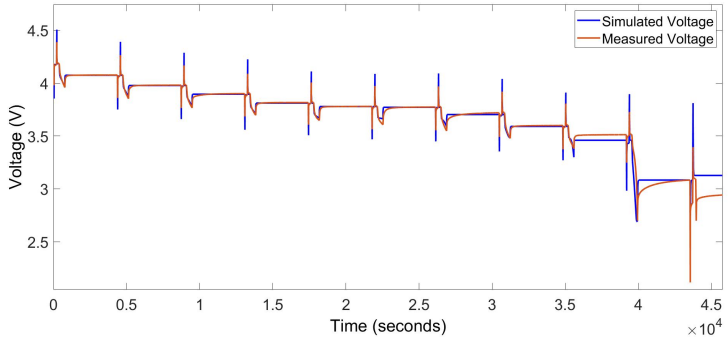

Figure A.4: HPPC test voltage for first-order Thevenin model at 318.15 K.

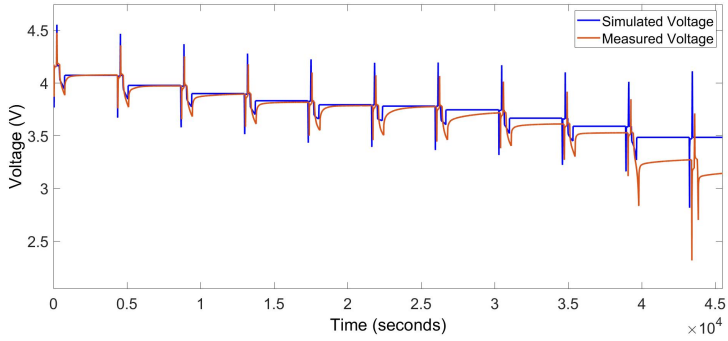

Figure A.5: HPPC test voltage for sescond-order Thevenin model at 288.15 K.

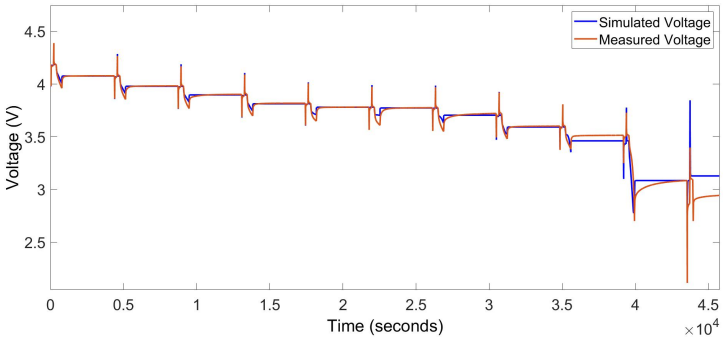

Figure A.6: HPPC test voltage for sescond-order Thevenin model at 318.15 K.